Research Square

Preprints are preliminary reports that have not undergone peer review.
They should not be considered conclusive, used to inform clinical practice,
or referenced by the media as validated information.

Dynamics of a Discrete-time Pioneer–climax Model

Nora Gilbertson (gilbertsonnora@gmail.com)
University of Washington https://orcid.org/0000-0001-7089-4036
Mark Kot
University of Washington

Research Article

Keywords: pioneer–climax model, difference equations, ecological succession, competitive exclusion, coexistence, bifurcations

Posted Date: February 11th, 2021

DOI: https://doi.org/10.21203/rs.3.rs-214803/v1

License: This work is licensed under a Creative Commons Attribution 4.0 International License.
Read Full License

Noname manuscript No.
(will be inserted by the editor)

Dynamics of a discrete-time pioneer–climax model

Nora Gilbertson[1,*] · **Mark Kot**[1]

Received: date / Accepted: date

Abstract We present a simple mathematical model for the dynamics of a successional pioneer–climax system using difference equations. Each population is subject to inter- and intraspecific competition; population density growth is dependent on the combined densities of both species. Nine different geometric cases, corresponding to different orientations of the zero-growth isoclines, are possible for this system. We fully characterize the long-term dynamics of the model for each of the nine cases, uncovering diverse sets of potential behaviors. Competitive exclusion of the pioneer species and exclusion of the climax species are both possible depending on the relative strength of competition. Stable coexistence of both species may also occur; in two cases, a coexistence state is destabilized through a Neimark–Sacker bifurcation and an attracting invariant circle is born. The invariant circle eventually disappears into thin air in a heteroclinic or homoclinic bifurcation, leading to the sudden transition of the system to an exclusion state. Neither global bifurcation has been observed in a discrete-time pioneer–climax model before. The homoclinic bifurcation is novel to all pioneer–climax models. We conclude by discussing the ecological implications of our results.

Keywords pioneer–climax model · difference equations · ecological succession · competitive exclusion · coexistence · bifurcations

* Corresponding author
E-mail: nmg421@uw.edu
ORCID 0000-0001-7089-4036

1 Department of Applied Mathematics, University of Washington Seattle, WA, USA

1 Introduction

In ecological succession, newly established habitat is initially composed of pioneer plants, hardy species that do best at low population densities and are able to colonize unpopulated environments (Dalling, 2019; Harper, 1977; Turner, 2001). Later in succession come climax species, which are strong competitors but poor colonizers (Harper, 1977; Turner, 2001). At low population densities, climax plants typically cannot persist on their own, and pioneer species act as nurse plants in a commensal interaction (Harper, 1977; Selgrade and Namkoong, 1990). As population density of the climax species increases, interaction dynamics become more competitive and the climax species tends to thrive (Pandolfi, 2019; Selgrade and Namkoong, 1990). In nature, there are many pairs of plants that interact in this manner. White bursage and creosote bush from the Sonoran Desert, a pioneer species and a climax species, are one such pair (McAuliffe, 1988).

There is a rich history of modeling pioneer–climax dynamics with systems of both differential and difference equations (Buchanan and Selgrade, 1995; Franke and Yakubu, 1994a,b; Kim and Marlin, 1999; Selgrade and Namkoong, 1990; Selgrade and Roberds, 1996, 1997; Sumner, 1996). In these models, the long-term behavior of both species depends on inter- and intraspecific competition, and each species reacts differently to these competitive effects. Most pioneer–climax models distinguish density-dependent effects from competition through use of a total-density variable, a linear combination of the population densities of both pioneer and climax species weighted by competitive effects. Competitive effects are thus dependent only on individual population densities. The models then assume that the per-capita replacement rate, or fitness, of each species is a function of the total-density variable, so that the species' response to density is modeled by this fitness function.

Pioneer species' fitness functions are monotonically decreasing functions of total density (Selgrade and Namkoong, 1990). Climax species, on the other hand, do poorly at low densities. As density increases, their fitness increases, until overcrowding at high densities results in a decrease in fitness (Selgrade and Namkoong, 1990), forming a one-hump function. Such fitness functions match ecological observations, incorporating the dependence of the climax species on the pioneer at low densities for resources such as shade or shelter (Harper, 1977; McAuliffe, 1988). This formulation also includes the pioneer species being generally outcompeted by the climax species as density increases (McAuliffe, 1988).

Initially, most researchers assumed that the eventual result of any pioneer–climax dynamical model would be pioneer exclusion, an assumption supported by model results and ecological theory (Franke and Yakubu, 1994a; Harper, 1977; Selgrade and Namkoong, 1990). Habitat disturbances that prevent a stable state with only climax species are likely to occur (Dalling, 2019; Tilman, 1988), but scientists believed an undisturbed system would always result in climax species dominance. Selgrade and Namkoong (1990) first demonstrated the possibility of long-term dynamics other than pioneer exclusion by finding a Hopf bifurcation that led to stable periodic behavior and coexistence.

After this seminal work, more evidence for a variety of steady-state behaviors emerged (Buchanan, 1999; Franke and Yakubu, 1994a,b; Kim and Marlin, 1999). Much of this research used differential equations (Buchanan and Selgrade, 1995; Cornejo-Pérez and Barradas, 2015; Kim and Marlin, 1999; Selgrade, 1994; Sumner, 1996). Studies that employed difference equations generally focused on analysis of the possible Neimark–Sacker bifurcation, the discrete-time equivalent of a Hopf bifurcation, or theoretical proof of exclusion and coexistence principles (Franke and Yakubu, 1994a,b; Selgrade and Namkoong, 1990, 1991; Selgrade and Roberds, 1996). From these initial studies, pioneer–climax research turned to studying how a forcing term, representing stocking or harvesting, may be able to restore stability in the system after a Hopf or period-doubling bifurcation has occurred (Buchanan and Selgrade, 1995; Selgrade, 1994, 1998; Selgrade and Roberds, 1996, 1998; Sumner, 1996, 1998). To this point, no one has undertaken a more general overview of the behavior of a simple pioneer–climax difference-equation model.

We aim to provide such an overview, in order to understand the full long-term dynamics of a discrete-time model for the first time. With this comprehensive analysis, we gain further insight into how difference-equation models may contrast with differential-equation models, and we shed light on the unique behaviors a discrete-time model may reveal.

We present a basic pioneer–climax difference-equation model using similar assumptions to prior studies. In Section 2, we describe the model and its development. In this section, we also nondimensionalize our model. Using a total-density variable, we separate inter- and intraspecific competition effects and model the fitness of each species as a function of the total-density variable. We use simple rational forms for both fitness functions that are constructed in keeping with earlier model assumptions and ecological theory.

In Section 3, we characterize the zero-growth isoclines that provide the framework for our stability analysis. We also present the fixed points, or equilibria, of our model, which occur at the intersection of the zero-growth isoclines. Nine different geometric configurations of the zero-growth isoclines occur, as in Buchanan's 1999 analysis using differential equations. These nine cases present scenarios of both competitive exclusion and coexistence.

We perform a steady-state analysis of the long-term behavior of the model in Section 4 and summarize the results of the stability analysis for all nine geometric cases. The full stability analysis is contained in Appendix A, Appendix B, and Appendix C.

In two of the above cases, Neimark–Sacker bifurcations occur. We examine these bifurcations in Section 5. In Section 6 we highlight a global bifurcation similar to the heteroclinic cycle found in the differential-equation model of Kim and Marlin (1999) as well as another global bifurcation, a homoclinic bifurcation, not previously found in pioneer–climax models. We also present numerical simulations that show the changing stabilities of the fixed points or limit cycles as the bifurcations occur.

In Section 7, we discuss the implications of our findings and frame how this work can motivate future research directions. Our results provide insight into the persistence of pioneer and climax plant species and highlight previously unobserved global behavior of discrete-time pioneer–climax models. The complete investigation presented here opens the door to new research as well, in particular setting the framework for examining pioneer–climax models in a spatial context. Notably, this would allow us to examine a spatial pioneer–climax model in the context of invasion ecology with flexibility in the dispersal kernels and the ability to distinguish between growth and dispersal stages. As climate change alters ecosystems and induces range shifts in many species, we may see more successional communities, making such insight highly valuable.

2 Model

2.1 Model Development

We consider a model where sufficient resources exist so that the per-capita replacement rates of the pioneer and climax species depend only on the total-density variable, a linear combination of interspecific and intraspecific competition.

This construction allows us to distinguish between a species' response to density and its response to competitive effects. Let P_t and C_t be the population densities of the pioneer and climax species at time t. The total-density variables for each species are

$$M_t = w_{11}\,P_t + w_{12}\,C_t, \tag{1a}$$

$$N_t = w_{21}\,P_t + w_{22}\,C_t, \tag{1b}$$

where w_{ij} denotes the competitive effect of species j on species i. We take species 1 to be the pioneer species and species 2 to be the climax species.

The interaction between species is modeled by the system of difference equations

$$P_{t+1} = f(M_t)\,P_t, \tag{2a}$$

$$C_{t+1} = g(N_t)\,C_t, \tag{2b}$$

where $f(M_t)$ and $g(N_t)$ are the per-capita replacement rates, or fitness functions. We omit consideration of survivorship from one generation to the next. Note that for population growth of either species in this discrete-time model its fitness function $f(M_t)$ or $g(N_t)$ must be greater than 1.

We assume that the pioneer species' fitness function $f(M_t)$ is a monotonically decreasing function with respect to density that has a single root $f(M_t) = 1$. To model the pioneer species' dynamics under this assumption, consider the fitness function

$$f(M_t) = \frac{R_1}{1 + aM_t}. \tag{3}$$

The net reproductive rate of the pioneer species, R_1, is assumed to be greater than one to reflect the pioneer species' ability to survive on its own at low densities. We group deleterious effects such as overcrowding into the positive parameter a, so that the pioneer species' fitness always decreases with increasing total density, as shown in Fig. 1a.

The climax species' fitness function $g(N_t)$ is a one-hump function of density with two roots $g(N_t) = 1$. Thus, for the climax species, we take

$$g(N_t) = \frac{R_2(1 + b_1 N_t)}{1 + b_2 N_t^2}. \tag{4}$$

As with the pioneer species, R_2 is the climax species' net reproductive rate. As the climax species require the pioneer species to facilitate growth at low densities, R_2 is assumed to be less than one. Beneficial effects from the pioneer species acting as nurse plant for the climax species at low densities are incorporated in the positive parameter b_1. The positive parameter b_2, multiplied by the square of the total density, measures deleterious effects on the population at high densities due to effects such as overcrowding. This gives the desired form of the climax fitness function, increasing at low densities before hitting a maximum and decreasing as total density grows (Fig. 1b). Thus, the fitness functions presented here match ecological theory on the per-capita replacement rates of pioneer and climax species (Harper, 1977; McAuliffe, 1988) as well as mathematical convention (Kim and Marlin, 1999; Selgrade and Namkoong, 1990) while maintaining a desirable simplicity.

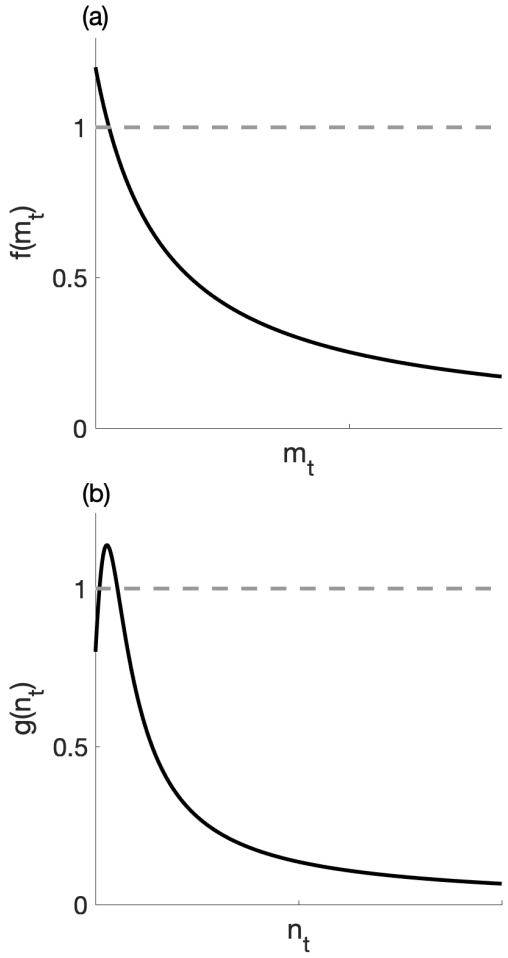

Fig. 1 Fitness functions for both species from the nondimensionalized model. **a**, the pioneer species' fitness function $f(m_t)$. **b**, the climax species' fitness function $g(n_t)$. The horizontal dashed gray lines indicate where the fitness function is equal to one, where the root(s) of the functions occur

2.2 Nondimensionalization

We scale the above system with respect to intraspecific competition, using the substitutions

$$x_t = w_{11}\,P_t, \tag{5a}$$

$$y_t = w_{22}\,C_t. \tag{5b}$$

This results in the new total-density variables

$$m_t = x_t + \left(\frac{w_{12}}{w_{22}}\right) y_t = x_t + v_2 y_t, \tag{6a}$$

$$n_t = \left(\frac{w_{21}}{w_{11}}\right) x_t + y_t = v_1 x_t + y_t, \tag{6b}$$

where v_1 and v_2 are now relative competition coefficients measuring the strength of interspecific competition proportionate to intraspecific competition.

We now have the nondimensional model

$$x_{t+1} = f(m_t)\, x_t = \frac{R_1 x_t}{1 + a m_t}, \tag{7a}$$

$$y_{t+1} = g(n_t)\, y_t = \frac{R_2(1 + b_1 n_t) y_t}{1 + b_2 n_t^2}. \tag{7b}$$

This scaling creates a model with fewer parameters, simplifying analysis significantly.

3 Zero-Growth Isoclines and Equilibria

To organize our analysis of the model given by Eq. 7, we use zero-growth isoclines as our framework. A zero-growth isocline is the set of points at which the population density of a species is not changing. Thus, in our discrete-time system, the zero-growth isoclines of the pioneer or climax species occur when $x_{t+1} = x_t = x$ or $y_{t+1} = y_t = y$ respectively. Under these conditions, our total density variables are $m_t = m = x + v_2 y$ and $n_t = n = v_1 x + y$. This gives us the equations

$$x = f(m)\, x, \tag{8a}$$

$$y = g(n)\, y. \tag{8b}$$

We see that Eq. 8a is satisfied either when $x = 0$ or when $f(m) = 1$. By construction, there is one root of the pioneer species' fitness function at $f(m) = 1$. Thus, in total there are two pioneer species zero-growth isoclines, the trivial one $x = 0$ and a nontrivial isocline where $f(m) = 1$ in the (x, y) plane. Both isoclines are linear.

Similarly, Eq. 8b has the solutions $y = 0$ or $g(n) = 1$. As the climax species' fitness function has two roots, we therefore have three zero-growth isoclines for the climax species. These are the trivial isocline $y = 0$ and two nontrivial isoclines from the solutions to $g(n) = 1$ in the (x, y) plane. The climax species' zero-growth isoclines are also linear.

Explicitly solving for the pioneer species' zero-growth isocline given by $f(m) = 1$ in terms of x and y yields the line

$$x = m^* - v_2 y, \tag{9}$$

where

$$m^* = \frac{R_1 - 1}{a}. \tag{10}$$

Doing the same for the climax species' zero-growth isoclines given by $g(n) = 1$ gives us the two lines

$$y = n_1^* - v_1 x, \tag{11a}$$

$$y = n_2^* - v_1 x, \tag{11b}$$

where

$$n_{1,2}^* = \frac{R_2 b_1 \pm \sqrt{R_2^2 b_1^2 - 4 b_2 (1 - R_2)}}{2 b_2}, \tag{12}$$

with n_1^* corresponding to the negative root and n_2^* the positive root.

A fixed point of Eq. 7 occurs at the intersection of two zero-growth isoclines, one isocline from each species, such that both populations are not changing over time. Given two zero-growth isoclines for the pioneer species and three for the climax species, there are six possible intersection points, and therefore six possible fixed points.

Four of these six, including the origin, are boundary equilibria and always exist. These boundary, or exclusion, equilibria are

$$E_1 = (x_1, y_1) = (0, 0), \tag{13}$$

the equilibrium at the origin where neither species persists,

$$E_2 = (x_2, y_2) = (m^*,\, 0), \tag{14}$$

the equilibrium where the pioneer species persists and excludes the climax species,

$$E_3 = (x_3, y_3) = (0,\, n_1^*), \tag{15}$$

the lower equilibrium on the y axis where the climax species persists but the pioneer species does not, and

$$E_4 = (x_4, y_4) = (0,\, n_2^*), \tag{16}$$

the upper equilibrium on the y axis where the climax species persists. The boundary equilibria result from the intersection of a trivial isocline ($x = 0$ or $y = 0$) with a zero-growth isocline of the other species.

Up to two interior equilibria may also exist. An interior coexistence state occurs when the nontrivial pioneer species' isocline crosses one of the nontrivial climax species' isoclines, i.e., when both $f(m) = 1$ and $g(n) = 1$. These equilibria are

$$E_5 = (x_5, y_5) = \left(\frac{m^* - v_2 n_1^*}{1 - v_1 v_2}, \frac{n_1^* - v_1 m^*}{1 - v_1 v_2}\right), \tag{17}$$

which results from the pioneer species' nontrivial zero-growth isocline crossing the lower climax species' nontrivial zero-growth isocline, and

$$E_6 = (x_6, y_6) = \left(\frac{m^* - v_2 n_2^*}{1 - v_1 v_2}, \frac{n_2^* - v_1 m^*}{1 - v_1 v_2}\right), \tag{18}$$

where the pioneer species' nontrivial zero-growth isocline crosses the upper climax species' nontrivial zero-growth isocline.

In order to analyze the equilibria and understand the long-term dynamics of our model (Eq. 7), we must consider the orientations of the isocline intersections that give rise to each equilibrium point. There are nine distinct geometric configurations of the zero-growth isoclines, some with interior equilibria and some without (Fig. 2, Fig. 3). The cases are distinguished from each other by restrictions on the parameter values. In particular, we fix all parameters but the relative competition coefficients v_1 and v_2, and obtain limits on v_1 and v_2 in terms of the other parameters for each case.

In three cases, the nontrivial isoclines do not cross each other and so only the four boundary equilibria E_{1-4} exist. These cases are shown in Fig. 2. In the six remaining cases, the nontrivial pioneer species' isocline crosses one or both of the nontrivial climax species' isoclines. The six configurations with interior equilibria are presented in Fig. 3.

4 Stability Analysis

For all nine cases, we now determine the stabilities of the four to six equilibria that occur in each case. To assess stability of an equilibrium, we can examine the eigenvalues of the Jacobian of Eq. 7 evaluated at that equilibrium. For asymptotic stability, both eigenvalues must be less than one in magnitude, i.e., $|\lambda_1| < 1$ and $|\lambda_2| < 1$. The general form of the Jacobian matrix for Eq. 7 is

$$J = \begin{bmatrix} f(m_t) + x_t f'(m_t)\frac{\partial m}{\partial x} & x_t f'(m_t)\frac{\partial m}{\partial y} \\ y_t g'(n_t)\frac{\partial n}{\partial x} & g(n_t) + y_t g'(n_t)\frac{\partial n}{\partial y} \end{bmatrix} = \begin{bmatrix} f(m_t) + x_t f'(m_t) & v_2 x_t f'(m_t) \\ v_1 y_t g'(n_t) & g(n_t) + y_t g'(n_t) \end{bmatrix}. \tag{19}$$

4.1 Boundary Equilibria

The eigenvalues of the Jacobian evaluated at each of the four boundary equilibria are given in Table 1. When $x = 0$ or $y = 0$, as in the boundary equilibria, an off-diagonal elements of the Jacobian J is zero. This allows us to simply read the eigenvalues off the diagonal of J. Additionally, for E_2 we may make the substitution $f(m) = 1$, as E_2 arises from the intersection of the isoclines $y = 0$ and $f(m) = 1$. Similarly, for $E_{3,4}$ we may say $g(n) = 1$, as these equilibria result from the intersections of $x = 0$ and the solutions to $g(n) = 1$.

The eigenvalues of all four boundary equilibria are real for any parameter values. We can also prove that the eigenvalues for all boundary equilibria are positive in all nine cases (see Appendix B for details).

Table 1 Boundary equilibria and their eigenvalues. Each equilibrium is generally represented by $E_i = (x_i, y_i)$

Fixed point	Eigenvalues
E_1	$\lambda_1 = R_1, \lambda_2 = R_2$
E_2	$\lambda_1 = g(v_1 x_2), \lambda_2 = 1 + x_2 f'(x_2)$
E_3	$\lambda_1 = f(v_2 y_3), \lambda_2 = 1 + y_3 g'(y_3)$
E_4	$\lambda_1 = f(v_2 y_4), \lambda_2 = 1 + y_4 g'(y_4)$

The origin is always a saddle point, as we assume $R_1 > 1$ and $R_2 < 1$. The stabilities of the other boundary equilibria are simple to determine in all cases by analyzing the eigenvalues. For E_{2-4}, we can establish whether λ_1 is greater or less than $+1$ by comparing where the non-zero component of the fixed point (i.e., x_2, y_3, or y_4) lands in relation to the root(s) where $g(v_1 x) = 1$ or $f(v_2 y) = 1$. This relation will be based on zero-growth isocline configuration for a given case. Similarly for E_{2-4}, λ_2 can be analyzed by determining the sign of the derivative of the fitness function evaluated at the given fixed point. If the derivative is positive, $\lambda_2 > 1$, and if it is negative, $\lambda_2 < 1$.

For the three cases in which only boundary equilibria exist, this completes our stability analysis. These three cases and the stabilities of their equilibria are shown in Fig. 2. The stabilities of the boundary equilibria in the six cases where at least one interior fixed point exists are shown in Fig. 3. A full stability analysis for the boundary equilibria in all nine cases is presented in Appendix B.

4.2 Interior Equilibria

The remaining six cases, where at least one interior fixed point occurs, are of significant interest given the potential for stable coexistence states. We classify the stabilities of the boundary fixed points in these cases as above, by analyzing the magnitude of their eigenvalues. For the interior equilibria, however, analyzing the magnitude of the eigenvalues is difficult, as the form of the eigenvalues is complicated and the eigenvalues may be complex. Thus, to determine the stabilities of the interior equilibria, we use the Jury conditions (Jury, 1964) applied to the Jacobian of Eq. 7 evaluated at each equilibrium point.

For this system, there are three Jury conditions that together prove stability of an equilibrium, given by

$$1 - \tau + \Delta > 0, \tag{20a}$$

$$1 + \tau + \Delta > 0, \tag{20b}$$

$$\Delta < 1, \tag{20c}$$

where τ and Δ are the trace and determinant of the Jacobian J. The first condition ensures there are no eigenvalues

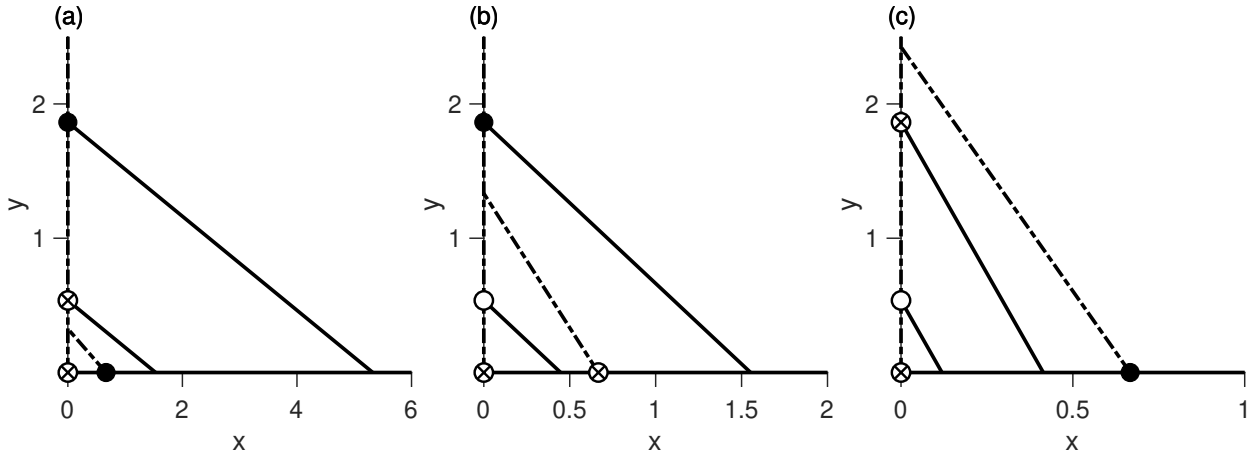

Fig. 2 Zero-growth isocline orientations and stabilities of fixed points for cases where only boundary fixed points exist. The dashed-dotted lines are the pioneer species' zero-growth isoclines; solid lines (including $y = 0$) are the climax species' zero growth isoclines. Solid black circles indicate asymptotically stable fixed points. Circles with crosses are saddle points, while open circles signify other unstable fixed points. For all cases, parameter values are $R_1 = 1.2, R_2 = 0.8, a = 0.3, b_1 = 0.6, b_2 = 0.2$. **a**, $v_1 = 0.35, v_2 = 2.05$. **b**, $v_1 = 1.2, v_2 = 0.5$. **c**, $v_1 = 4.5, v_2 = 0.275$

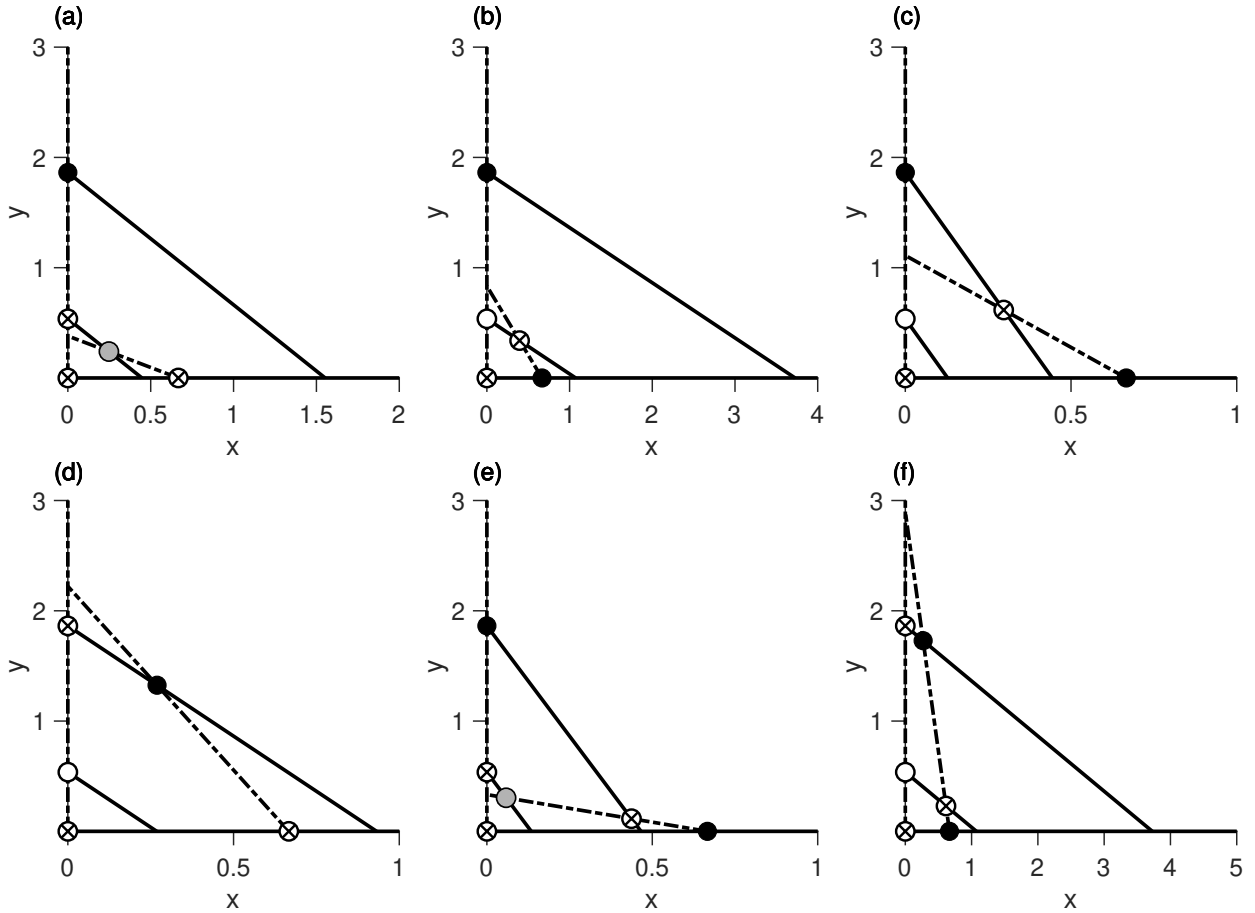

Fig. 3 Zero-growth isocline configurations and stabilities of equilibria for cases where interior equilibria occur. The dashed-dotted lines are the pioneer species' zero-growth isoclines; solid lines (including $y = 0$) are the climax species' zero growth isoclines. Parameter values for all cases are $R_1 = 1.2, R_2 = 0.8, a = 0.3, b_1 = 0.6, b_2 = 0.2$. The same classification system as in Fig. 2 applies; gray shaded circles represent equilibria that undergo bifurcations. **a** and **b**, one interior equilibrium results from the crossing of the pioneer zero-growth isocline and the lower climax zero-growth isocline. **a**, $v_1 = 1.2, v_2 = 1.75$; **b**, $v_1 = 0.5, v_2 = 0.8$. **c** and **d**, one interior equilibrium results from crossing the upper climax zero-growth isocline. **c**, $v_1 = 4.2, v_2 = 0.6$; **d**, $v_1 = 2, v_2 = 0.3$. **e** and **f**, two interior equilibria occur. **e**, $v_1 = 4, v_2 = 2$; **f**, $v_1 = 0.5, v_2 = 0.23$

greater than $+1$, the second that there are no eigenvalues less than -1. The third condition guarantees that no complex eigenvalues lie outside the unit circle.

Violating any of the Jury conditions as parameter values change will result in the equilibrium point changing stability via a local bifurcation. Violating the first Jury condition leads to a transcritical bifurcation. Violating the second Jury condition results in a flip, or period-doubling, bifurcation. If the third condition is violated, a Neimark–Sacker bifurcation will occur. This is the discrete-time analog of a Hopf bifurcation. By testing the Jury conditions on Jacobian (19) evaluated at the interior equilibrium point(s), for all six cases with coexistence states, we classify the stabilities of the interior equilibria as shown in Fig. 3.

For every case, the first Jury condition is either always satisfied or never satisfied for any parameter values within the case's bounds. Thus, there are no transcritical bifurcations for either coexistence fixed point while that fixed point remains within the interior of the first quadrant. However, the interior fixed point will shift toward the x axis if v_1 is varied and the y axis if v_2 is varied. There are critical v_1 and v_2 values that distinguish each geometric case from the others, and precisely at these critical values the interior fixed point hits one of the axes, colliding with one of the boundary equilibria in the process. Therefore, transcritical bifurcations do occur as the interior fixed point passes through the boundary equilibria, corresponding to a change in geometric case. This results in the coexistence equilibria exiting the first quadrant, leading to negative population densities.

The results of the transcritical bifurcations that occur are evident from Fig. 2 and Fig. 3. Compare, for example, Fig. 2c and Fig. 3c. As v_2 decreases, the pioneer species' isocline (dashed-dotted line) in Fig. 3c shifts, its y-intercept increasing, and the interior equilibrium E_5 moves toward the y axis. Eventually, E_5 collides with the y axis at E_4, and the equilibria exchange stabilities. The previously stable equilibrium E_4 becomes a saddle point, and E_5 passes out of the first quadrant as an asymptotically stable fixed point. As v_2 decreases further, the pioneer species' isocline lies fully above the two climax species' isoclines, and we are now in the case shown in Fig. 2c, where we see that E_4 is indeed a saddle point and there is no interior fixed point in the first quadrant.

The second Jury condition is never violated, and so there are no period-doubling bifurcations. More precisely, we can prove, through use of Descartes' Rule of Signs (Descartes, 1886), that all real eigenvalues of Jacobian (19) are positive for both interior equilibria in all cases. This rules out violation of the second Jury condition. This result is in contrast to several other studies that demonstrated period-doubling bifurcations in their discrete-time pioneer–climax models (Joshi and Blackmore, 2010; Selgrade, 1998; Selgrade and Roberds, 1997, 1998).

For all four cases in which equilibrium E_6 exists (Fig. 3c, 3d, 3e, and 3f), we can prove that all eigenvalues of the Jacobian evaluated at E_6 are strictly real. We can prove the same for two of the cases with equilibrium E_5 (Fig. 3b and 3f). Thus, we do not analyze the third Jury condition at all for E_6, nor for E_5 in two cases, as this condition applies to complex eigenvalues. We determine stabilities of the relevant interior equilibria in these cases by again using Descartes' Rule of Signs (Descartes, 1886), to find the number of eigenvalues that are above and below $+1$. As we also know that our real roots are positive, this information is all we require to classify the stabilities of the interior fixed point(s) in these cases.

In the remaining two cases in which E_5 occurs, one with only E_5 (Fig. 3a) and one with both interior equilibria (Fig. 3e), we cannot show that the eigenvalues at E_5 are always real. Numerically, we find that the eigenvalues may be real or complex for different parameter values. Thus, for these two cases we fix R_1, R_2, a, b_1, and b_2 and analyze the third Jury condition to find a region in the (v_1, v_2) plane for which equilibrium E_5 is asymptotically stable. The parameters v_1 and v_2 were selected to highlight how relative competition coefficients affect stability. Competition is the main underlying factor influencing the density of both pioneer and climax species, as seen in the construction of our model. Therefore, the competition parameters were a natural choice to analyze.

The determinant of the Jacobian evaluated at E_5 is

$$\Delta = \big(1 + x_5 f'(m)\big)\big(1 + y_5 g'(n)\big) - v_1 v_2 x_5 y_5 f'(m) g'(n), \tag{21}$$

with $m = x_5 + v_2 y_5$ and $n = v_1 x_5 + y_5$. After substituting in the explicit forms of the equilibrium and derivatives, it is possible to solve the equation $\Delta = 1$ for v_2 as a function of v_1 (or vice versa). Thus, for both cases we can get a curve for the third Jury condition that defines the region of stability for E_5 in the (v_1, v_2) plane. These curves are shown in Fig. 4. Above and to the left of the solid curve, E_5 is asymptotically stable. Crossing the solid curve violates the third Jury condition and destabilizes E_5 via a Neimark–Sacker bifurcation. For the explicit form of the curves for the third Jury condition, as well as a full stability analysis of the interior fixed points, see Appendix C.

In all, four of the six cases with interior equilibria have an asymptotically stable coexistence state for at least some parameter values. In two of these cases, equilibrium E_6 is always asymptotically stable. The other two have limited parameter regions where equilibrium E_5 is asymptotically stable (Fig. 4). Even after E_5 has become unstable in these two cases, an attracting invariant circle is born from the Neimark–Sacker bifurcation that destabilized E_5. We will now examine this local bifurcation in more detail.

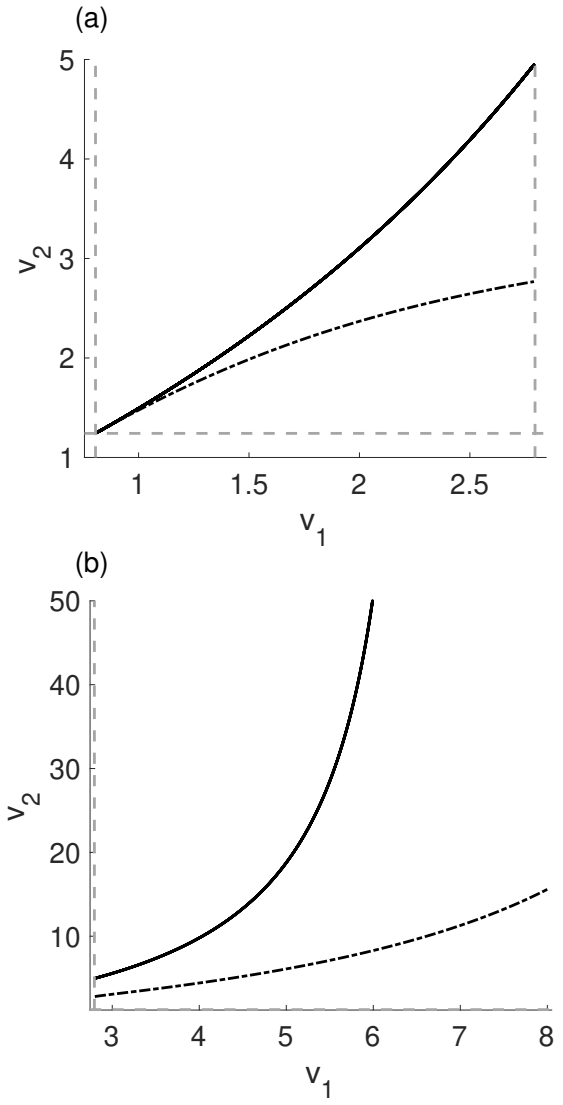

Fig. 4 Stability region for equilibrium E_5, defined by the curves in (v_1, v_2) parameter space where bifurcations occur. In both cases, E_5 is stable for parameter values above and to the left of the solid curve given by $\Delta = 1$; crossing this curve results in a loss of stability via a Neimark–Sacker bifurcation and the birth of an invariant circle. The lower dashed-dotted curves are the boundaries at which the global bifurcations occur; crossing the dashed-dotted curve results in the abrupt disappearance of the invariant circle. **a**, the first case corresponding to Fig. 3a with a heteroclinic bifurcation. The global bifurcation curve was found by using the bisection method to calculate, for a given v_1, the v_2 value for which a trajectory starting on the unstable manifold of E_2 ended at, or very near to, E_3, such that the unstable manifold of E_2 connected with the stable manifold of E_3. **b**, the second case corresponding to Fig. 3e with a homoclinic bifurcation. The global bifurcation curve for this case was found by using the bisection method to determine, for a given v_1, the v_2 value for which a trajectory starting on the unstable manifold of E_6 returned to E_6, such that the unstable and stable manifolds of E_6 connected to form a homoclinic connection. The dashed gray lines in each panel indicate the boundaries on v_1 and v_2 such that we are in the appropriate geometric case, i.e., that the isoclines intersect in the appropriate configuration. Parameter values for both cases are $R_1 = 1.2, R_2 = 0.8, a = 0.3, b_1 = 0.6, b_2 = 0.2$

5 Neimark–Sacker Bifurcation

In two geometric cases we violate the third Jury condition for equilibrium E_5 by having a pair of complex conjugate eigenvalues exit the unit circle. These cases correspond to Fig. 3a and 3e. For the remainder of this section and the next (Section 6), we will refer to them as the first case and the second case.

In both cases, for parameter values above and to the left of the curve $\Delta = 1$, equilibrium E_5 is asymptotically stable (Fig. 4). As v_2 decreases and crosses this boundary, the equilibrium point loses stability via a Neimark–Sacker bifurcation and an attracting quasiperiodic solution, commonly known as an invariant circle, emerges. As v_2 continues to decrease, the invariant circle grows larger. The attracting invariant circle for a variety of v_2 values can be seen in Fig. 5 for the first case and in Fig. 6 for the second case.

As we have noted, loss of stability via a Neimark–Sacker bifurcation for fixed point E_5 occurs as the relative competition coefficient v_2 decreases for fixed v_1. Thus, as intraspecific competition in the climax species grows stronger relative to the competitive effect of the climax species on the pioneer species, the equilibrium destabilizes. Equivalently, if v_2 were fixed, the equilibrium loses stability as v_1 increases. Biologically, this corresponds to the competitive effect of the pioneer species on the climax species increasing relative to the competitive effect of the pioneer species on itself. In either context, v_1 increasing or v_2 decreasing, the fixed point E_5 is destabilized when a species' competitive effect on the climax species grows stronger relative to its competitive effect on the pioneer species. In place of the fixed point, an attracting quasiperiodic solution arises, resulting in stable population fluctuations.

To fully characterize the Neimark–Sacker bifurcation, we must consider the possibility of resonance. Resonance cases occur when the complex conjugate eigenvalues $\lambda, \overline{\lambda}$ of our Jacobian exit the unit circle through a root of unity such that $\lambda = e^{2\pi i p/q}$ and $\overline{\lambda} = e^{-2\pi i p/q}$, where p and q are both positive integers and p/q is known as the rotation number (Aronson et al., 1982; Whitley, 1983). This phenomenon is called strong resonance if $q \leq 4$ and weak resonance for $q \geq 5$ (Lauwerier, 1986; Whitley, 1983). The bifurcation that occurs in a resonance case does not lead to the birth of an invariant circle; phase-locked periodic solutions or more complicated behaviors arise instead (Arnol'd, 1977; Kuznetsov, 2004; Lauwerier, 1986).

In both cases with the Neimark–Sacker bifurcation, the eigenvalues of the Jacobian are precisely on the unit circle for any (v_1, v_2) pair that lies on the curve $\Delta = 1$ (Fig. 4). Thus, if the eigenvalues are located at roots of unity for any such (v_1, v_2) pair, resonance occurs for those parameter values. To check for cases of resonance, we numerically calculate the eigenvalues of the Jacobian for all (v_1, v_2) pairs on

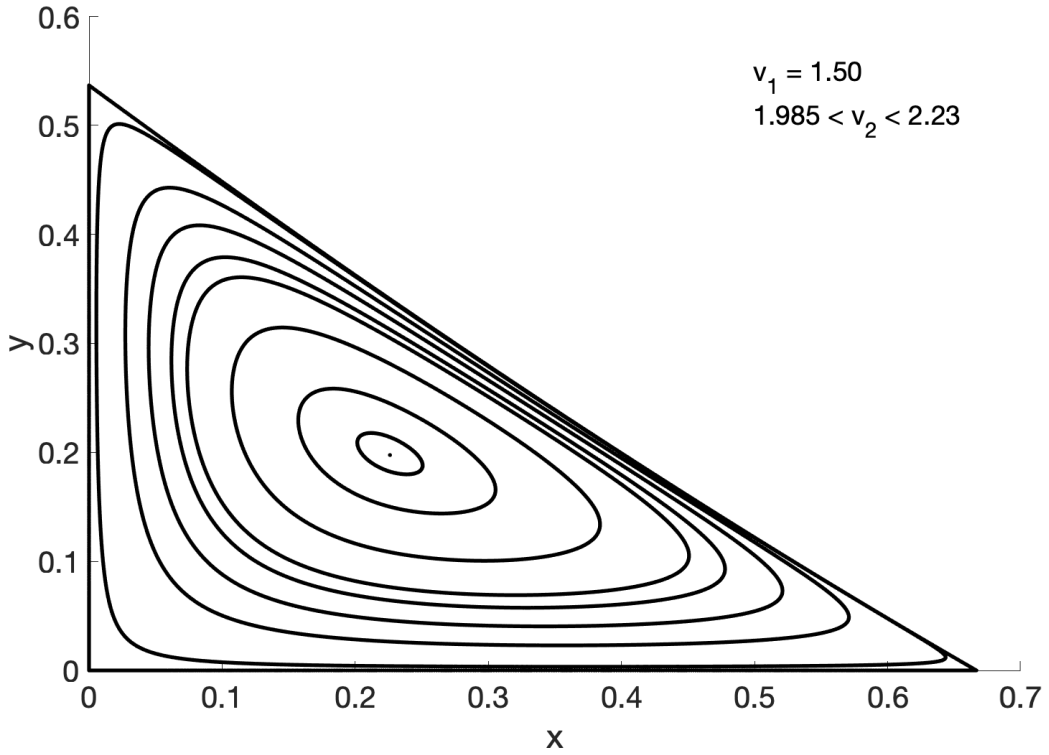

Fig. 5 Growth of the invariant circle as v_2 decreases from 2.23 to just above 1.985 in the first case with a Neimark–Sacker bifurcation. The point in the middle of the invariant circles is E_5 for $v_2 = 2.23$, when E_5 is asymptotically stable. We ran the system for 50,000 iterations; the final 15,000 iterations were plotted for ten v_2 values. Parameter values are $R_1 = 1.2, R_2 = 0.8, a = 0.3, b_1 = 0.6, b_2 = 0.2$

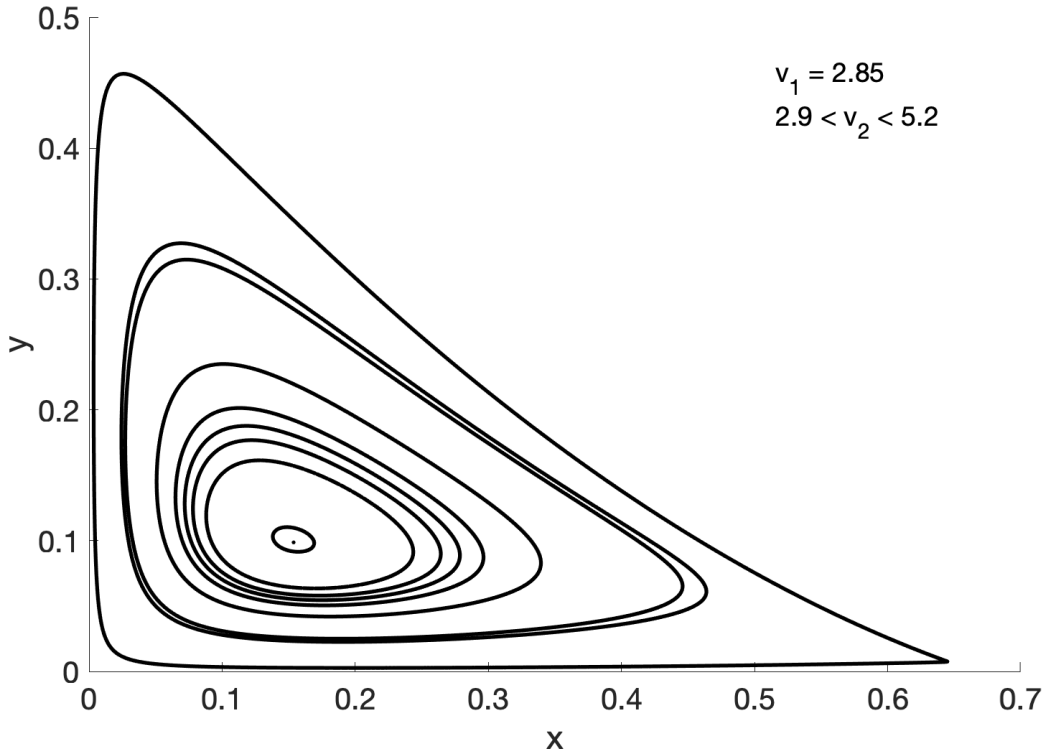

Fig. 6 Growth of the invariant circle in the second case as v_2 decreases from 5.2 to 2.9. The single point in the middle of the invariant circles is E_5 for $v_2 = 5.2$, when E_5 is asymptotically stable. The system was run for 1,000,000 iterations; the final 200,000 iterations were plotted for ten v_2 values. This number of iterations was necessary to fill in the invariant circle for some v_2 values for which the system had nearly rational rotation numbers. Other parameter values are $R_1 = 1.2, R_2 = 0.8, a = 0.3, b_1 = 0.6, b_2 = 0.2$

the curve $\Delta = 1$, i.e., parameters for which the eigenvalues lie on the unit circle, and isolate the rotation number p/q. If the rotation number is rational, we have a p/q resonance (Aronson et al., 1982).

In both cases with a Neimark–Sacker bifurcation, the rotation numbers as our eigenvalues pass through the unit circle are very small. This precludes the possibility of strong resonance, as the smallest rotation number that would lead to strong resonance is $p/q = 1/4$.

There is no solid evidence for weak resonance either, although this could be due to numerical inaccuracy in calculating the rotation numbers. For some parameter values, particularly in the second case with a Neimark–Sacker bifurcation, it takes many thousands of iterations to densely fill the invariant circle. This indicates we may have rotation numbers that are very close to, but not quite, rational. Weak resonance cases give rise to phase-locked periodic orbits, but there is no evidence of periodic solutions in a bifurcation diagram. Instead, the bifurcation diagram shows only densely filled invariant circles or fixed points (Fig. 7, Fig. 8). Thus, if phase-locking occurs, it is likely for an orbit of extremely high period that is unnoticeable in numerical calculations.

In a discrete-time system, it is not uncommon after a Neimark–Sacker bifurcation for the invariant circle to eventually deform or for further bifurcations to occur, leading to a strange attractor (Aronson et al., 1982; Curry and Yorke, 1978; Neubert and Kot, 1992; Selgrade and Namkoong, 1991; Selgrade and Roberds, 1996). Such behavior has been shown specifically in pioneer–climax discrete-time models (Selgrade and Namkoong, 1991; Selgrade and Roberds, 1996), as well as in a continuous-time pioneer–climax model (Selgrade, 1994). We do not observe such behavior here. Instead, in both cases with a Neimark–Sacker bifurcation, a global bifurcation occurs as the invariant circle grows larger. We now turn to investigate these global bifurcations.

6 Global Bifurcations

As can be seen in Fig. 5 and Fig. 6, in both cases with a Neimark–Sacker bifurcation the invariant circle grows closer and closer to the axes as v_2 decreases. Additionally, the invariant circle appears to approach some limiting curve with negative slope within the first quadrant. For a critical v_2 value, the invariant circle abruptly vanishes, leaving no attractor in the interior at all, in what is known as a dangerous global bifurcation (Thompson et al., 1994). The mechanism by which this disappearance of the invariant circle occurs is different in the two bifurcation cases, and we have two types of global bifurcation resulting in the blue-sky disappearance of an invariant circle.

6.1 Heteroclinic Bifurcation

Recall that in the first case (Fig. 3a, Fig. 5), there are three saddle points on the boundaries. These occur at E_1 at the origin, E_2 on the x-axis, and E_3, the lower fixed point on the y-axis. In this case, for a critical v_2 value, a heteroclinic cycle forms between the three saddle points. The invariant circle runs into the heteroclinic cycle and instantaneously vanishes. Thus, we have the blue-sky disappearance of an invariant circle due to a heteroclinic bifurcation.

The heteroclinic cycle that forms is relatively simple and is shown in Fig. 9b. The y axis is the unstable manifold of E_3 and the stable manifold of E_1, so a heteroclinic connection is formed moving from E_3 into E_1 along the y axis. Similarly, the x axis is the unstable manifold of E_1 and the stable manifold of E_2; so the portion of the x axis between E_1 and E_2 forms a heteroclinic connection as well. Finally, the unstable manifold of E_2 connects with the stable manifold of E_3, finishing off a triangular heteroclinic cycle between E_1, E_2 and E_3. Prior to and after the global bifurcation, the invariant manifolds of E_2 and E_3 do not intersect (Fig. 9a, 9c).

Numerically, this last heteroclinic connection between E_2 and E_3 appears to be a linear or near-linear connection (Fig. 9), suggesting these manifolds may coincide, or at the very least are nearly indistinguishable from one another. Kim and Marlin (1999) found in a differential-equation pioneer–climax model that, for the same geometric zero-growth isocline configuration, there was a critical parameter value for which the unstable manifold of E_2 and the stable manifold of E_3 coincided. While their continuous-time model was different from our discrete-time model, it offers support to the idea that these manifolds may indeed coincide; however, we leave an analytic proof for the future.

6.2 Homoclinic Bifurcation

There are also three saddle points in the second case (Fig. 3e, Fig. 6), two on the boundaries at E_1 (the origin) and E_3 (the y-axis) and one just off of the x-axis at E_6. However, a heteroclinic cycle does not form between these three saddle points as in the first case; a homoclinic connection forms between the stable and unstable manifolds of the coexistence equilibrium E_6 instead (Fig. 10b, Fig. 11). The invariant circle runs into the homoclinic connection for a particular v_2 value, resulting in the blue sky disappearance of an invariant circle due to a homoclinic bifurcation.

The stable manifold of the interior equilibrium E_6 winds very close to the x and y axes but never intersects either axis, precluding a heteroclinic connection between E_6 and the origin (Fig. 11). Nevertheless, due to this closeness, we see the invariant circle grow very near to both axes. The invariant circle does not come close to the lower equilibrium on the y axis E_3, however, even very close to the point at which the

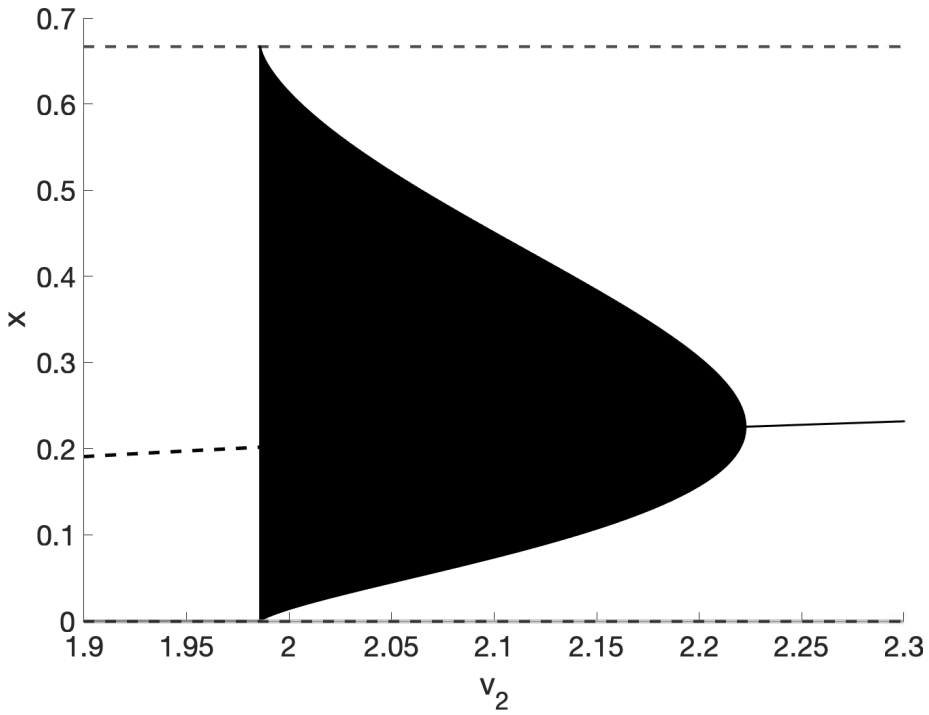

Fig. 7 Bifurcation diagram for the first case with bifurcations, showing the x coordinates of the attractors and other fixed points. Dashed lines represent saddle points or other unstable fixed points; solid lines represent asymptotically stable fixed points. The black dashed line on top of the gray solid line at $x = 0$ is included to show there are both stable and unstable fixed points with coordinate $x = 0$. As v_2 decreases, we see the birth of an invariant circle due to a Neimark–Sacker bifurcation. All x values on the invariant circle are mapped, such that for a single v_2 value there are many values of x. The invariant circle grows as v_2 decreases further until its sudden disappearance in a global bifurcation as the invariant circle runs into a heteroclinic cycle between the three saddle points of this case. Parameter values are $R_1 = 1.2, R_2 = 0.8, a = 0.3, b_1 = 0.6, b_2 = 0.2, v_1 = 1.5$

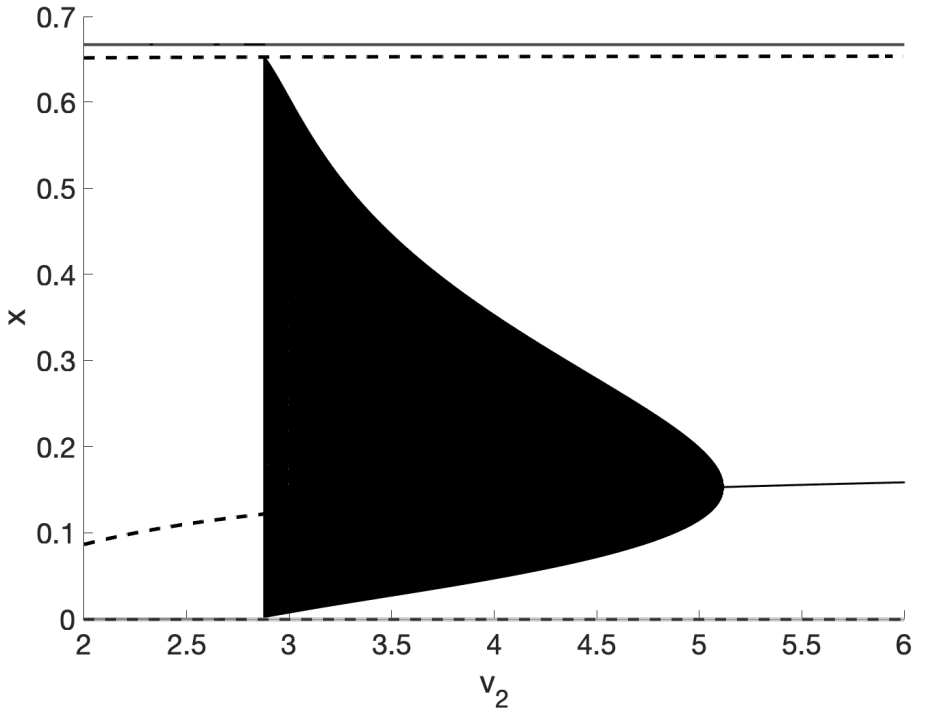

Fig. 8 Bifurcation diagram of the second case showing the x coordinates of the attractors and other fixed points. Dashed lines show saddle points or other unstable fixed points; solid lines represent asymptotically stable fixed points. The black dashed line on top of the solid gray line at $x = 0$ shows there are both stable and unstable fixed points at $x = 0$. As with the first case, as v_2 decreases an invariant circle is born via a Neimark–Sacker bifurcation, eventually abruptly vanishing in a global bifurcation. Parameter values are $R_1 = 1.2, R_2 = 0.8, a = 0.3, b_1 = 0.6, b_2 = 0.2, v_1 = 2.85$

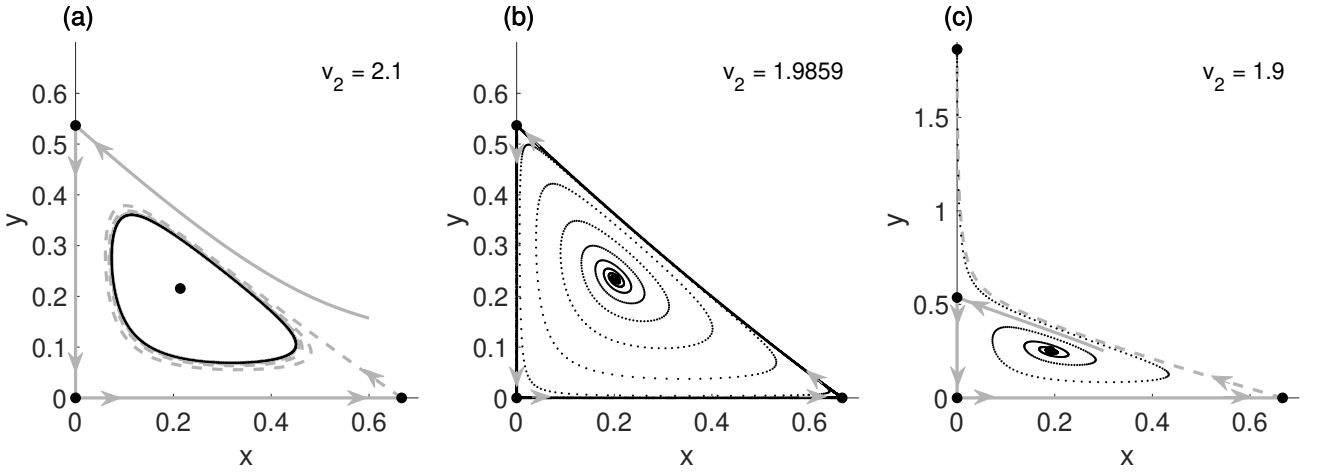

Fig. 9 Behavior of the system before, at, and after the heteroclinic bifurcation in the first case with bifurcations. Solid gray lines are stable manifolds, dashed gray lines are unstable manifolds. The axes are also invariant manifolds and form heteroclinic connections between E_1 and E_2 on the x axis and E_1 and E_3 on the y axis. Large black points are equilibria, trajectories of the system with an initial condition near E_5 are shown with smaller black points. The arrows indicate the direction of travel along the manifold. **a**, prior to the global bifurcation, the unstable manifold from E_2 passes below the stable manifold of E_3 and winds onto the attracting invariant circle. **b**, at the point of global bifurcation, a heteroclinic cycle forms and the unstable and stable manifolds of E_2 and E_3 link together to complete the cycle. **c**, after the global bifurcation, the heteroclinic connection is broken and no stable coexistence state exists. Almost all trajectories go to E_4 on the y axis, save for solutions starting on the stable manifold of E_3 or on the axes between E_1 and E_2 or between E_1 and E_3. Parameter values are $R_1 = 1.2, R_2 = 0.8, a = 0.3, b_1 = 0.6, b_2 = 0.2, v_1 = 1.5$

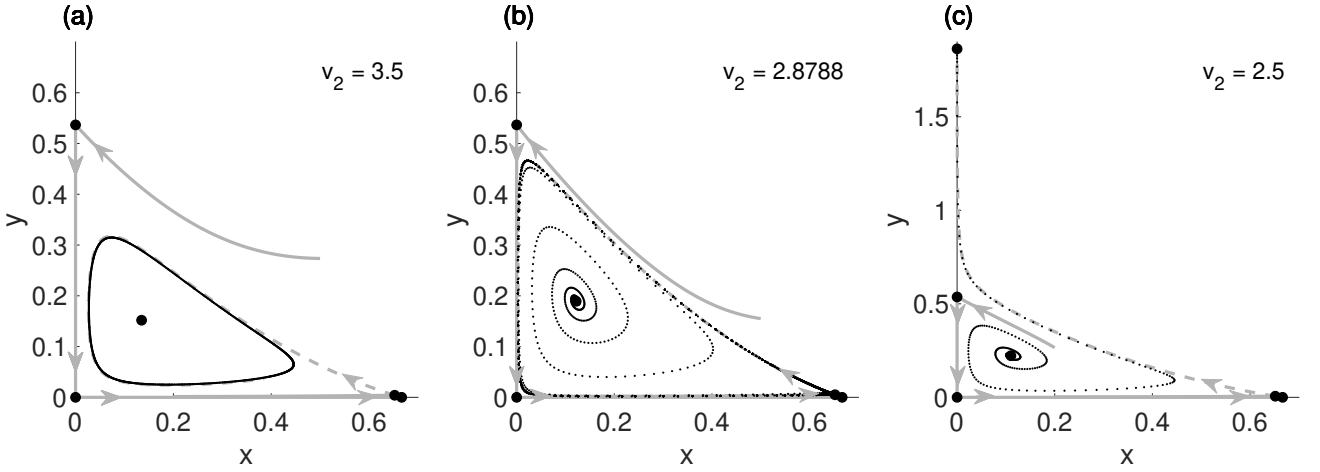

Fig. 10 Behavior of the system before, at, and after the homoclinic bifurcation in the second case with bifurcations. Solid gray lines are stable manifolds, dashed gray lines are unstable manifolds. The axes are again invariant manifolds with heteroclinic connections between E_1 and E_2 on the x axis and E_1 and E_3 on the y axis. Large black points represent equilibria, trajectories of the system starting near E_5 are shown with smaller black points. Arrows indicate direction of travel along the manifolds. **a**, prior to the global bifurcation, the unstable manifold from interior equilibrium E_6 passes below the stable manifold from E_3 on the y axis and winds onto the attracting invariant circle. **b**, at the point of global bifurcation, a homoclinic connection forms between the stable and unstable manifolds of E_6, passing very close to the invariant manifolds on the axes. **c**, after the global bifurcation, no stable coexistence state exists and the homoclinic connection has been broken. Almost all trajectories go either to E_4 on the y axis (shown here) or E_2 on the x axis. Parameter values are $R_1 = 1.2, R_2 = 0.8, a = 0.3, b_1 = 0.6, b_2 = 0.2, v_1 = 2.85$

global bifurcation occurs. This can be seen by noting that the maximum height, or y coordinate, of the largest invariant circle is significantly lower in Fig. 6 than in Fig. 5. In addition to the fact that the manifolds of E_6 do not intersect the manifolds of E_1 or E_3, this behavior is further indicative of the differences between the heteroclinic cycle of the first case and the homoclinic connection in this second case.

6.3 Behavior Near the Global Bifurcations

In both cases, as v_2 decreases the invariant circle grows larger until it is pushed up against the heteroclinic cycle or homoclinic connection (Fig. 5, Fig. 6). At a critical v_2 value, the circle can grow no more, constrained by the invariant manifolds that have formed a heteroclinic cycle or homoclinic connection (Fig. 9b, Fig. 10b), and the invariant cir-

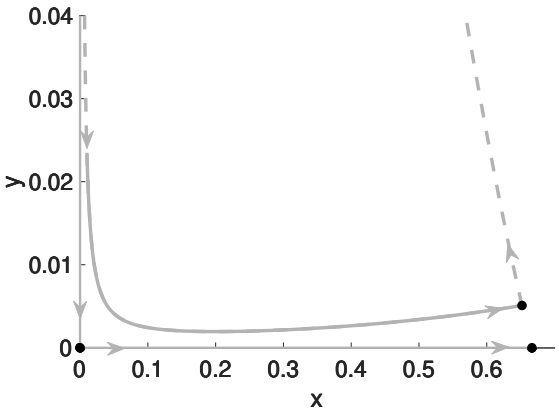

Fig. 11 A magnified view of the lower part of the homoclinic connection in the second case with bifurcations. Here, the loop between the stable and unstable manifolds of E_6 is clear, and we more easily see that the invariant manifolds of E_6 do not intersect the manifolds on the axes of E_1 or E_2. Solid gray lines are stable manifolds, dashed gray lines are unstable manifolds, and points are equilibria. Arrows indicate direction of travel along the manifolds. Parameter values are $R_1 = 1.2, R_2 = 0.8, a = 0.3, b_1 = 0.6, b_2 = 0.2, v_1 = 2.85$, and $v_2 = 2.878800266186866$

cle vanishes into thin air. The disappearance of the invariant circle corresponds to crossing the dashed-dotted line from above in Fig. 4. We see in Fig. 4 that for fixed v_1 an invariant circle exists only in the space between the solid line, when the invariant circle appears due to a Neimark–Sacker bifurcation, and the dashed-dotted line, which shows the point of global bifurcation when the invariant circle vanishes.

The disappearance of the invariant circle due to a global bifurcation is starkly apparent in a bifurcation diagram (Fig. 7, Fig. 8). In both cases, we see the edges of the invariant circle, represented by the minimum and maximum x values of the invariant circle, run into the saddle point at E_2 or E_6, depending on the case, and the two saddle points E_1 and E_3 with coordinate $x = 0$.

The blue sky disappearance of an invariant circle due to a heteroclinic bifurcation is a global bifurcation not previously observed in a discrete-time pioneer–climax model, though Kim and Marlin (1999) noted this bifurcation for the first case in continuous time. This is, however, the first time that anyone has observed the disappearance of an invariant circle due to a homoclinic bifurcation in a pioneer–climax system, whether in discrete or continuous time.

We have already noted that in both cases with bifurcations, E_5 was destabilized and an attracting quasiperiodic solution arose as a species' competitive effect on the climax species grew stronger relative to its effect on the pioneer species. Now, we see that if this competitive effect on the climax species becomes stronger still, the attracting orbit vanishes entirely, leaving no stable coexistence state at all. This is, perhaps, a ready conclusion to draw from observing the growth of the invariant circle. As v_2 decreases and competitive effect on the climax species becomes stronger, populations are regularly driven very close to either $x = 0$ or $y = 0$, such that a small stochastic effect on the populations may easily drive one species to extinction.

7 Discussion

As climate change affects ecosystems, causing effects from range shifts to increased habitat disturbances, successional communities are likely to become more common (Chen et al., 2011; Lenoir et al., 2008; Seidl et al., 2017). In this paper, we introduced a simple discrete-time pioneer–climax model where the species' interaction dynamics are built upon principles of ecological succession. We characterized the long-term dynamics of the model in the first in-depth analytical stability analysis of a discrete-time pioneer–climax system, and the stability results were supported by numerical simulations. Our analysis is organized around nine geometric cases that are distinguished by different parameter regimes, corresponding to limits on the relative competition coefficients v_1 and v_2. The model results in a diverse set of long-term behaviors among the nine different cases, some of which are novel to a discrete-time pioneer–climax model. These behaviors were robust to other parameter sets.

Of these nine geometric configurations, six cases have an asymptotically stable climax-exclusion state in which the pioneer survives (Fig. 2a, 2c, Fig. 3b, 3c, 3e, and 3f). For a long time, researchers assumed the asymptotic result of an undisturbed pioneer–climax system was pioneer exclusion (Selgrade and Namkoong, 1990; Harper, 1977). Many pioneer–climax models have since shown that pioneer exclusion is not the only possible long-term behavior, but this was done primarily through proofs of the stabilities of coexistence states (e.g., Kim and Marlin (1999); Selgrade and Roberds (1996); Sumner (1996)). The existence of asymptotically stable climax-exclusion states was largely ignored in these analyses.

It is interesting, however, that in a majority of the nine parameter regimes the system does indeed have an asymptotically stable climax-exclusion state. This result tells us that even in an undisturbed environment, under some (perhaps limited) circumstances the pioneer species could not just coexist with the climax species, but it could even outcompete the climax species. The only cases in which a stable pioneer-only state was not present was for moderate values of v_1, i.e., when the effect of the pioneer on the climax species is is relatively close to the effect of the pioneer species on itself.

Five of the six cases with an asymptotically stable climax exclusion state also have other asymptotically stable states (Fig. 2a, Fig. 3b, 3c, 3e, and 3f). In addition to these five, the first case with bifurcations has multiple stable states for parameter values prior to the heteroclinic bifurcation

(Fig. 3a). We therefore have six cases in total with multiple stable states that the system may tend to, depending on initial conditions and parameter values.

While the existence of multiple stable states is an ongoing debate in ecological theory, increasing evidence suggests that multiple stable states may indeed exist in nature (Beisner et al., 2003; Folke et al., 2004; Petraitis, 2013; Scheffer and Carpenter, 2003; Schröder et al., 2005). Being able to determine conditions under which an ecosystem may tend toward one stable state or another may be of particular interest in conservation and ecosystem management. Using this model, we provide a framework for understanding such conditions.

In all, the model presents four different cases, Fig. 3a, 3d, 3e, and 3f, with stable coexistence states. In two of these cases, the interior fixed point is asymptotically stable for all relevant parameter values. In each of the other two cases, however, two bifurcations, one local and one global, change the nature of the coexistence state. For some parameter values, the coexistence state is an asymptotically stable fixed point. The Neimark–Sacker bifurcation that occurs in both cases destabilizes the interior fixed point and gives rise to an attracting quasi-periodic invariant circle, and a global bifurcation later causes the attractor to vanish entirely.

While many studies of pioneer–climax models have shown the existence and stability of the attractor that arises after a Hopf (or Neimark–Sacker) bifurcation (Selgrade and Namkoong, 1990; Selgrade and Roberds, 1996; Sumner, 1996, 1998), only one considered the persistence of the attractor. One continuous-time system noted the abrupt disappearance of the attractor (Kim and Marlin, 1999), but in only one geometric case. This corresponds to our first case with bifurcations and the associated heteroclinic bifurcation. In the second case with bifurcations, two coexistence states occur. We discovered that the formation of a homoclinic connection between the invariant manifolds of one coexistence equilibrium (E_6) can result in the blue-sky disappearance of the attracting invariant circle that arose after the other coexistence equilibrium E_5 was destabilized. Thus, there are two cases for which the behavior of the system can change precipitously, causing a loss of any stable coexistence state and a sudden transition of the system to a new exclusion state. Knowledge of the conditions under which an attracting coexistence state vanishes may be important for ecosystem management.

While the structure of our model is simple, with rational fitness functions, we believe that this model captures the major dynamics of a pioneer–climax system and provides valuable insight into an inherently successional system. However, two species do not exist in a vacuum, and there are many more layers of interaction dynamics that could be taken into account, as in Joshi and Blackmore's (2010) higher-dimensional model. To confirm the realism of this two-dimesional model, in the future it would be beneficial to compare our model predictions with data from pioneer–climax systems. Such data may be challenging to gather, given the long timescales involved in ecological succession. Additionally, the number of parameters in this model may make parameter estimation difficult.

A limitation of our model stems from a lack of survival from one generation to the next, despite many pioneer and climax species living longer than the duration of a single generation. One simple way of accounting for survivorship is to add small positive linear terms, $s_1 x_t$ or $s_2 y_t$, to our model, where s_1 and s_2 represent the probability of surviving to the next generation. This would shift our per capita replacement rates (Fig. 1) upwards by a constant amount. Based on preliminary analytical and numerical exploration, the additional terms will not significantly change the behavior of our model, though some restrictions on the relative strength of survivorship may be necessary to ensure stability.

Spatiotemporal dynamics of successional communities are increasingly relevant in both conservation and invasion ecology. Through spatiotemporal modeling of a pioneer-climax system, we can approach problems like determining the critical patch size for population persistence or quantifying the rate of invasion into a new habitat by calculation of a species' spreading speed. Additionally, moving habitat models can inform us whether or not populations can keep pace with climate-induced range shifts. With such germane and interesting problems, future work should focus on incorporating spatial components into our model.

After the many initial studies into the basic dynamics of pioneer–climax models and the potential for reversing bifurcations and restoring stability in those models (e.g., Kim and Marlin (1999); Selgrade and Namkoong (1990); Selgrade and Roberds (1997); Sumner (1996)), research on pioneer–climax systems has indeed made the shift to spatiotemporal models, but it has largely focused on reaction-diffusion models. Much of this research has focused on proving the existence of traveling waves (Brown et al., 2005; Buonomo and Rionero, 2009; Cao and Weng, 2017; Huang and Weng, 2013; Yu et al., 2013; Yuan and Zou, 2010). Other studies have looked at Turing and Hopf bifurcations in reaction-diffusion systems (Buchanan, 1999; Liu and Wei, 2011). Two isolated studies have examined spreading speed within a reaction-diffusion context (Cao and Weng, 2017; Weng and Zou, 2014).

These studies provide a valuable starting point in the analysis of spatiotemporal dynamics of pioneer–climax systems. However, the problems mentioned above on critical patch size and moving habitat models are wholly unexamined, and only two studies have examined spreading speed (Cao and Weng, 2017; Weng and Zou, 2014). Furthermore, reaction-diffusion models are limited in their ecological re-

alism, as dispersal is often non-diffusive and growth, particularly in plants, is frequently seasonal (Lewis et al., 2016; Lutscher, 2019).

Using the discrete-time model presented here, however, we can develop a more ecologically realistic spatiotemporal integrodifference equation model to examine the same problems. These models have the benefit of separating growth and dispersal, and they take long-distance dispersal into account in a way reaction-diffusion models do not. With flexible dispersal kernels and separation of growth and dispersal phases, a common feature in plant populations, integrodifference equations provide a more ecologically realistic method of examining some of these spatial issues in invasions and conservation (Kot and Schaffer, 1986; Lewis et al., 2016; Lutscher, 2019).

Before moving to these more complex questions, it is critical that we understand the dynamics of the underlying foundational models, like the one analyzed here. Our work in analyzing this discrete-time system not only advances our knowledge of stationary pioneer–climax dynamics, but also paves the way for situating our model within a spatial context. With this framework, we have the ability to examine how these species will persist, invade new habitat, and survive in an ever-changing environment.

Declarations

Funding

The authors declare they have received no funding supporting this work.

Conflicts of Interest

The authors declare that they have no conflicts of interest.

Availability of data and material

Not applicable.

Code availability

Matlab version R2019a was used to create all figures.

Authors' contributions

Nora Gilbertson: formal analysis, writing – original draft, writing – review and editing. Mark Kot: conceptualization, supervision, writing – review and editing.

Ethics approval

Not applicable.

Consent to participate

Not applicable.

Consent for publication

Not applicable.

References

Arnol'd VI (1977) Loss of stability of self-oscillations close to resonance and versal deformations of equivariant vector fields. Funct Anal its Appl 11:85–92

Aronson DG, Chory MA, Hall GR, McGehee RP (1982) Bifurcations from an invariant circle for two-parameter families of maps of the plane: A computer assisted study. Commun Math Phys 83:303–354

Beisner BE, Haydon DT, Cuddington K (2003) Alternative stable states in ecology. Front Ecol Environ 1:376–382

Brown S, Dockery J, Pernarowski M (2005) Traveling wave solutions of a reaction diffusion model for competing pioneer and climax species. Math Biosci 194:21–36

Buchanan JR (1999) Asymptotic behavior of two interacting pioneer/climax species. Fields Inst Commun 21:51–63

Buchanan JR, Selgrade JF (1995) Constant and periodic rate stocking and harvesting for Kolmogorov-type population interaction models. Rocky Mt J Math 25:76–85

Buonomo B, Rionero S (2009) Linear and nonlinear stability thresholds for a diffusive model of pioneer and climax species interaction. Math Methods Appl Sci 32:811–824

Cao J, Weng P (2017) Single spreading speed and traveling wave solutions of a diffusive pioneer–climax model without cooperative property. Commun Pure Appl Anal 16:1405–1426

Chen I, Hill JK, Ohlemüller R, Roy DB, Thomas CD (2011) Rapid range shifts of species associated with high levels of climate warming. Science 333:1024–1026

Cornejo-Pérez O, Barradas I (2015) Dynamics of a pioneer–climax species model with migration. Appl Math Model 39:6568–6579

Curry JH, Yorke JA (1978) A transition from Hopf bifurcation to chaos: Computer experiments on maps in R^2. In: Markley NG, Martin JC, Perrizo W (eds) The structure of attractors in dynamical systems, Springer-Verlag, Berlin, pp 48–68

Dalling JM (2019) Pioneer species. In: Fath BD (ed) Encyclopedia of ecology, Elsevier, Amsterdam, pp 181–184

Descartes R (1886) [1637] La géométrie. Hermann, A., Paris

Folke C, Carpenter SR, Walker B, Scheffer M, Elmqvist T, Gunderson L, Holling CS (2004) Regime shifts, resilience, and biodiversity in ecosystem management. Annu Rev Ecol Evol Syst 35:557–581

Franke JE, Yakubu AA (1994a) Exclusion principles for density-dependent discrete pioneer–climax models. J Math Anal Appl 187:1019–1046

Franke JE, Yakubu AA (1994b) Pioneer exclusion in a one-hump discrete pioneer–climax competitive system. J Math Biol 32:771–787

Harper JL (1977) Population biology of plants. Academic Press, London

Huang Y, Weng P (2013) Traveling wavefronts of a diffusive competing pioneer and climax system with delays. Math Comput Model 57:2532–3548

Joshi Y, Blackmore D (2010) Bifurcation and chaos in higher dimensional pioneer–climax systems. Int Electron J Pure Appl Math 1:303–337
Jury EI (1964) Theory and application of the z-transform method. Wiley, New York
Kim H, Marlin JA (1999) Solutions of a pioneer–climax model. Can Appl Math Q 7:143–158
Kot M, Schaffer WM (1986) Discrete-time growth-dispersal models. Math Biosci 80:109–136
Kuznetsov YA (2004) Elements of applied bifurcation theory. Springer, New York
Lauwerier HA (1986) Two-dimensional iterative maps. In: Holden AV (ed) Chaos, Princeton Univ. Press, Princeton, pp 58–95
Lenoir J, Gégout JC, Marquet PA, de Ruffray P, Brisse H (2008) A significant upward shift in plant species optimum elevation during the 20th century. Science 320:1768–1771
Lewis MA, Petrovskii SV, Potts JR (2016) The mathematics behind biological invasions. Springer, Switzerland
Liu J, Wei J (2011) Bifurcation analysis of a diffusive model of pioneer and climax species interaction. Adv Differ Equ 2011:1–11
Lutscher F (2019) Integrodifference equations in spatial ecology. Springer, Switzerland
McAuliffe JR (1988) Markovian dynamics of simple and complex desert plant communities. Am Nat 131:459–490
Neubert MG, Kot M (1992) The subcritical collapse of predator populations in discrete-time predator–prey models. Math Biosci 110:45–66
Pandolfi JM (2019) Succession. In: Fath BD (ed) Encyclopedia of ecology, Elsevier, Amsterdam, pp 616–623
Petraitis PS (2013) Multiple stable states in natural ecosystems. Oxford University Press, Oxford
Scheffer M, Carpenter SR (2003) Catastrophic regime shifts in ecosystems: Linking theory to observation. Trends Ecol Evol 18:648–656
Schröder A, Persson L, De Roos AM (2005) Direct experimental evidence for alternative stable states: A review. Oikos 110:3–19
Seidl R, Thom D, Kautz M, Martin-Benito D, Peltoniemi M, Vacchiano G, Wild J, Ascoli D, Petr M, Honkaniemi J, Lexer MJ, Trotsiuk V, Mairota P, Svoboda M, Fabrika M, Nagel TA, Reyer CPO (2017) Forest disturbances under climate change. Nat Clim Chang 7:395–402
Selgrade JF (1994) Planting and harvesting for pioneer–climax models. Rocky Mt J Math 24:293–310
Selgrade JF (1998) Using stocking or harvesting to reverse period-doubling bifurcations in discrete population models. J Differ Equ Appl 4:163–183
Selgrade JF, Namkoong G (1990) Stable periodic behavior in a pioneer–climax model. Nat Resour Model 4:215–227
Selgrade JF, Namkoong G (1991) Population interactions with growth rates dependent on weighted densities. In: Busenberg S, Martelli M (eds) Differential equations models in biology, epidemiology and ecology, Springer-Verlag, Berlin, pp 247–256
Selgrade JF, Roberds JH (1996) Lumped-density population models of pioneer–climax type and stability analysis of Hopf bifurcations. Math Biosci 135:1–21
Selgrade JF, Roberds JH (1997) Period-doubling bifurcations for systems of difference equations and applications to models in population biology. Nonlinear Anal Theory Methods Appl 29:185–199
Selgrade JF, Roberds JH (1998) Reversing period-doubling bifurcations in models of population interactions using constant stocking or harvesting. Can Appl Math Q 6:207–231
Sumner S (1996) Hopf bifurcation in pioneer–climax competing species models. Math Biosci 137:1–24
Sumner S (1998) Stable periodic behavior in pioneer–climax competing species models with constant rate forcing. Nat Resour Model 11:155–171
Thompson JMT, Stewart HB, Ueda Y (1994) Safe, explosive, and dangerous bifurcations in dissipative dynamical systems. Phys Rev E 49:1019–1027
Tilman D (1988) Plant strategies and the dynamics and structure of plant communities. Princeton University Press, Princeton
Turner IM (2001) The ecology of trees in the tropical rain forest. Cambridge University Press, Cambridge
Weng P, Zou X (2014) Minimal wave speed and spread speed of competing pioneer and climax species. Appl Anal 93:2093–2110
Whitley D (1983) Discrete dynamical systems in dimensions one and two. Bull London Math Soc 15:177–217
Yu X, Weng P, Huang Y (2013) Traveling wavefronts of competing pioneer and climax model with nonlocal diffusion. Abstr Appl Anal 2013:1–12
Yuan Z, Zou X (2010) Co-invasion waves in a reaction diffusion model for competing pioneer and climax species. Nonlinear Anal Real World Appl 11:232–245

Appendix A Preliminary Organization and Derivatives for the Jacobian

Throughout all appendices, we will refer to the fixed points as E_1–E_6, and their individual components as x_1–x_6 and y_1–y_6. Eq. 13–Eq. 18 provide the explicit forms of the equilibria, which are used only in rare cases. We now drop all time-dependent notation, as we are analyzing fixed points (x, y) that, by definition, do not change over time. In all of our calculations, we consider only nonnegative x and y, and therefore nonnegative m and n. All parameters are positive.

We first recall that there are nine different geometric cases (illustrated in Fig. 2 and Fig. 3) for this system, and up to six equilibria that exist in each case. The parameter restrictions bounding each of the nine cases are summarized in Table 2. In three cases, only boundary fixed points exist. In the other six cases, one or both interior fixed points occur in addition to the boundary equilibria. Stability analyses for the boundary fixed points are relatively straightforward, and each boundary fixed point can be analyzed individually and its stability classified for each case based on the parameter restrictions from Table 2. The interior fixed points present more of a challenge, and are examined on a case-by-case basis. The inequalities presented in Table 2 are also heavily used in classifying the stabilities for the interior fixed points. The stabilities of the fixed points for all nine cases are summarized in Table 3.

To begin our stability analyses, we first present some general results that we will use extensively. After this initial setup is complete, we proceed to the boundary fixed points and classify the stability of each boundary fixed point for all nine cases by examining the magnitudes of the eigenvalues of Jacobian (19). We finally move to the interior fixed-points and lay out a few general results that are specific to the interior fixed points and the eigenvalues of Jacobian (19) evaluated at the interior fixed points. Our stability analyses for the interior fixed points proceed on a case-by-case basis, and for each case, we use the Jury conditions (Eq. 20)

Table 2 Parameter restrictions for each of the nine geometric cases. For the six parameter regimes with at least one interior fixed point, these conditions are the same as those for existence of the interior fixed point(s) in the first quadrant. A dash in the 'Case' column indicates that no specific label has been assigned to that case. A dash in the 'Interior fixed point' column indicates no interior fixed point exists for that parameter regime. There is no Condition 3 for the three parameter regimes with no interior equilibria, as that condition was derived by restricting an interior fixed point to be within the first quadrant

Figure	Case	Interior fixed point	Condition 1	Condition 2	Condition 3
Fig. 2a	–	–	$v_1 < n_1^*/m^*$	$v_2 > m^*/n_1^*$	–
Fig. 2b	–	–	$n_1^*/m^* < v_1 < n_2^*/m^*$	$m^*/n_2^* < v_2 < m^*/n_1^*$	–
Fig. 2c	–	–	$v_1 > n_2^*/m^*$	$v_2 < m^*/n_2^*$	–
Fig. 3a	a	E_5	$n_1^*/m^* < v_1 < n_2^*/m^*$	$v_2 > m^*/n_1^*$	$1 < v_1 v_2$
Fig. 3b	b	E_5	$v_1 < n_1^*/m^*$	$m^*/n_2^* < v_2 < m^*/n_1^*$	$v_1 v_2 < 1$
Fig. 3c	c	E_6	$v_1 > n_2^*/m^*$	$m^*/n_2^* < v_2 < m^*/n_1^*$	$1 < v_1 v_2$
Fig. 3d	d	E_6	$n_1^*/m^* < v_1 < n_2^*/m^*$	$v_2 < m^*/n_2^*$	$v_1 v_2 < 1$
Fig. 3e	e	E_5 and E_6	$v_1 > n_2^*/m^*$	$v_2 > m^*/n_1^*$	$1 < v_1 v_2$
Fig. 3f	f	E_5 and E_6	$v_1 < n_1^*/m^*$	$v_2 < m^*/n_2^*$	$v_1 v_2 < 1$

Table 3 Stability of each equilibrium point in the nine different cases. A dash indicates the fixed point does not exist in the first quadrant for that parameter regime

Figure	E_1	E_2	E_3	E_4	E_5	E_6
Fig. 2a	saddle point	stable node	saddle point	stable node	–	–
Fig. 2b	saddle point	saddle point	unstable node	stable node	–	–
Fig. 2c	saddle point	stable node	unstable node	saddle point	–	–
Fig. 3a	saddle point	saddle point	saddle point	stable node	bifurcations	–
Fig. 3b	saddle point	stable node	unstable node	stable node	saddle point	–
Fig. 3c	saddle point	stable node	unstable node	stable node	–	saddle point
Fig. 3d	saddle point	saddle point	unstable node	saddle point	–	stable node
Fig. 3e	saddle point	stable node	saddle point	stable node	bifurcations	saddle point
Fig. 3f	saddle point	stable node	unstable node	saddle point	saddle point	stable node

and Descartes' Rule of Signs (Descartes, 1886) to bound the eigenvalues of the Jacobian evaluated at the given interior fixed point.

A.1 Derivatives for the Jacobian

Recall that a fixed point is asymptotically stable if both eigenvalues of Jacobian (19) evaluated at the fixed point are less than 1 in magnitude. If stability of a fixed point is classified through use of the Jury conditions, the trace τ and determinant Δ of the Jacobian are important quantities for consideration. When evaluated at a fixed point, our Jacobian matrix (19) has elements containing the derivatives of the fitness functions, including the particular quantities $1 + x_i f'(m_i)$ and $1 + y_i g'(n_i)$, where x_i and y_i are the coordinates of the fixed point and m_i and n_i are also evaluated at that fixed point. Before beginning our stability analyses, it is useful to present some general results pertaining to the derivatives of the fitness functions and these key quantities.

First, we explicitly calculate the forms of the derivatives $f'(m)$ and $g'(n)$, where

$$f'(m) = \frac{-aR_1}{(1+am)^2} < 0 \tag{22}$$

for all m. We will write $g'(n)$ in a way that is particularly useful by first considering the expression

$$\begin{aligned} 1 - g(n) &= \frac{1 + b_2 n^2 - R_2 (1 + b_1 n)}{1 + b_2 n^2} \\ &= \frac{b_2 (n - n_1^*)(n - n_2^*)}{1 + b_2 n^2}, \end{aligned} \tag{23}$$

where we factored the numerator to obtain the second equality. Differentiating both sides with respect to n, we find

$$g'(n) = \frac{-b_2\left[(n-n_1^*)+(n-n_2^*)\right]}{1+b_2n^2} + \frac{2b_2^2 n\,(n-n_1^*)\,(n-n_2^*)}{(1+b_2n^2)^2}, \tag{24}$$

which may be either positive or negative. In particular, note that for $n=n_1^*$, $g'(n)>0$, and when $n=n_2^*$, $g'(n)<0$.

Next, note that

$$\frac{\partial}{\partial x}\left[f(m)x\right] = f(m)+xf'(m)\frac{\partial m}{\partial x} = f(m)+xf'(m), \tag{25}$$

which is the upper-left entry in Jacobian matrix (19) for this system. Explicitly calculating this quantity, we find

$$\frac{\partial}{\partial x}\left[f(m)x\right] = \frac{R_1(1+av_2y)}{\left[1+a(x+v_2y)\right]^2} > 0. \tag{26}$$

Thus, for all nonnegative x and y,

$$f(m)+xf'(m) > 0. \tag{27}$$

At fixed points E_2, E_5, and E_6, $f(m)=1$, and so Eq. 27 simplifies even further to

$$1+x_if'(m_i) > 0 \tag{28}$$

for $i=2,5,6$, $m_i = x_i+v_2y_i$.

We now consider the lower-right entry of the Jacobian matrix. As above,

$$\frac{\partial}{\partial y}\left[g(n)y\right] = g(n)+yg'(n)\frac{\partial n}{\partial y} = g(n)+yg'(n). \tag{29}$$

Unlike Eq. 27, we do not prove this quantity is positive in general. However, it is positive at each of the four equilibria E_3–E_6 for which $y\neq 0$ and $g(n)=1$. We now prove this statement for each of the four fixed points individually.

At E_3, recall that $y=n=n_1^*$. Substituting this relation into Eq. 29 and using Eq. 24 to simplify the derivative, we obtain

$$g(n)+yg'(n) = 1+\frac{b_2n_1^*(n_2^*-n_1^*)}{1+b_2\left(n_1^*\right)^2} > 0, \tag{30}$$

as $n_2^* > n_1^*$.

Similarly, at E_4, $y=n=n_2^*$. Again substituting this relation into Eq. 29, we find

$$g(n)+yg'(n) = 1-\frac{b_2n_2^*(n_2^*-n_1^*)}{1+b_2\left(n_2^*\right)^2} = \frac{1+b_2n_1^*n_2^*}{1+b_2\left(n_2^*\right)^2} > 0, \tag{31}$$

after finding a common denominator and simplifying.

For E_5, we have $y=y_5$ and $n=v_1x_5+y_5=n_1^*$. Using the same process as above,

$$g(n)+yg'(n) = 1+\frac{b_2y_5(n_2^*-n_1^*)}{1+b_2\left(n_1^*\right)^2} > 0. \tag{32}$$

Finally, at E_6, $y=y_6$ and $n=v_1x_6+y_6=n_2^*$. Instead of using the fact that $g(n_2^*)=1$, we substitute the explicit form of $g(n_2^*)$, which has the same denominator as that of $g'(n_2^*)$. We find that

$$g(n)+yg'(n) = \frac{R_2(1+b_1n_2^*)-b_2y_6(n_2^*-n_1^*)}{1+b_2\left(n_2^*\right)^2}. \tag{33}$$

The denominator is positive, so if the numerator is positive then Eq. 33 is positive as desired. Considering the numerator of Eq. 33, we begin by simplifying $n_2^*-n_1^*$, yielding

$$\begin{aligned} &R_2(1+b_1n_2^*)-b_2y_6(n_2^*-n_1^*) \\ &= R_2(1+b_1n_2^*)-y_6\sqrt{R_2^2b_1^2-4b_2(1-R_2)}. \end{aligned} \tag{34}$$

For convenience, denote

$$c = \sqrt{R_2^2b_1^2-4b_2(1-R_2)} \tag{35}$$

and substitute $n_2^* = v_1x_6+y_6$ into Eq. 34 to obtain

$$\begin{aligned} &R_2\left[1+b_1(v_1x_6+y_6)\right]-cy_6 \\ &= R_2(1+b_1v_1x_6)+y_6(R_2b_1-c). \end{aligned} \tag{36}$$

Finally, using

$$\begin{aligned} n_1^* &= \frac{R_2b_1-c}{2b_2} \\ \implies 2b_2n_1^* &= R_2b_1-c, \end{aligned} \tag{37}$$

we can rewrite Eq. 36 as

$$R_2(1+b_1v_1x_6)+y_6(2b_2n_1^*), \tag{38}$$

which is clearly positive. Thus, the numerator of Eq. 33 is positive and therefore Eq. 33 is positive.

We have just shown that $g(n)+yg'(n)>0$ when evaluated at each of the fixed points E_3–E_6, i.e.,

$$1+y_ig'(n_i) > 0 \tag{39}$$

for $i=3,4,5,6$, $n_i = v_1x_i+y_i$.

Appendix B Stability of Boundary Fixed Points

With these general quantities and inequalities laid out, we now establish the stability of the four boundary fixed points for all nine parameter regimes. Refer to Table 1 for the eigenvalues for each fixed point E_1–E_4.

First, note that all eigenvalues are positive and real for the boundary fixed points. It is clear that the eigenvalues for E_1 are positive and real, as the eigenvalues are the populations' net reproductive rates, which must be positive. Furthermore, as the fitness functions $f(m)$ and $g(n)$ are always real and greater than zero, it is evident that $\lambda_1 > 0$ and is real for E_2–E_4. Next, consider λ_2 as given in Table 1. As demonstrated in Appendix A by Eq. 28, Eq. 30, and Eq. 31, we see that $\lambda_2 > 0$ for E_2–E_4. Thus, both eigenvalues are positive for all four boundary fixed points. To prove stability of E_1–E_4, it is therefore sufficient to show whether each eigenvalue λ_1 and λ_2 is greater or less than $+1$.

With the knowledge that $f'(m) < 0$ always, $g'(n_1^*) > 0$, $g'(n_2^*) < 0$, and the results shown in Appendix A, we may continue with proving the stability of the boundary fixed-points for the nine cases shown in Fig. 2 and Fig. 3.

B.1 Stability of Trivial Extinction State E_1

As mentioned in Subsection 4.1, the equilibrium E_1 at the origin is always a saddle point, as the associated eigenvalues of the Jacobian are $R_1 > 1$ and $0 < R_2 < 1$.

B.2 Stability of Climax-Exclusion State E_2

By construction of the climax fitness function $g(n)$, there are two roots n, n_1^* and n_2^*, where $g(n) = 1$. For values of n below and above those roots, $g(n) < 1$, and for values of n between the roots, $g(n) > 1$ (see Fig. 1b).

Consider $n = v_1 x$. Then, $g(n) = g(v_1 x)$. The two roots where $g(v_1 x) = 1$ are given by

$$v_1 x_\alpha = n_1^* \implies x_\alpha = n_1^*/v_1, \tag{40a}$$

$$v_1 x_\beta = n_2^* \implies x_\beta = n_2^*/v_1. \tag{40b}$$

Thus, the value of $\lambda_1 = g(v_1 x_2)$ depends on where x_2 falls in relation to x_α and x_β from Eq. 40. Let $n_2 = v_1 x_2$. We see that

$$x_2 < x_\alpha \implies n_2 < n_1^* \implies \lambda_1 = g(n_2) < 1, \tag{41a}$$

$$x_2 > x_\beta \implies n_2 > n_1^* \implies \lambda_1 = g(n_2) < 1, \tag{41b}$$

$$x_\alpha < x_2 < x_\beta \implies n_1^* < n_2 < n_2^* \implies \lambda_1 = g(n_2) > 1. \tag{41c}$$

Observe that x_α and x_β are the x-intercepts of the two zero-growth isoclines where $g(n) = 1$, while x_2 is the x-intercept of the zero-growth isocline $f(m) = 1$. Thus, we can read off the magnitude of λ_1 straight from the configuration of the zero-growth isoclines for a particular case.

Recall that $\lambda_2 = f(x_2) + x_2 f'(x_2) = 1 + x_2 f'(x_2)$. By Eq. 28, $\lambda_2 > 0$. As $f'(m) < 0$ for all m, $\lambda_2 < 1$.

Combining our analysis for both eigenvalues, we see that stability depends on λ_1, as $0 < \lambda_2 < 1$. E_2 will be a stable node if the nontrivial pioneer zero-growth isocline intercepts the x-axis to the left or right of both nontrivial climax zero-growth isoclines ($x_2 < x_\alpha$ or $x_2 > x_\beta$). It will be a saddle point if the nontrivial pioneer zero-growth isocline intercepts the x-axis between the two nontrivial climax zero-growth isoclines ($x_\alpha < x_2 < x_\beta$). See Fig. 2 and Fig. 3 for details. The stability of E_2 for each of the nine cases is summarized in Table 3.

B.3 Stability of Pioneer-Exclusion States E_3 and E_4

Now, consider the construction of the pioneer fitness function. There is one root m where $f(m) = 1$. For values of m below this root, $f(m) > 1$, and for values of m above this root, $f(m) < 1$ (see Fig. 1a).

Take $m = v_2 y$. Then $f(m) = f(v_2 y)$. The root where $f(v_2 y) = 1$ is

$$v_2 y_\alpha = \frac{R_1 - 1}{a} = m^* \implies y_\alpha = m^*/v_2. \tag{42}$$

As with E_2, for E_3 the value of $\lambda_1 = f(v_2 y_3)$ depends on the size of y_3 relative to y_α. Similarly, for E_4 the value of $\lambda_1 = f(v_2 y_4)$ depends on the size of y_4 relative to y_α. Let $m_3 = v_2 y_3$ and $m_4 = v_2 y_4$.

For E_3,

$$y_3 < y_\alpha \implies m_3 < m^* \implies \lambda_1 = f(m_3) > 1, \tag{43a}$$

$$y_3 > y_\alpha \implies m_3 > m^* \implies \lambda_1 = f(m_3) < 1. \tag{43b}$$

For E_4,

$$y_4 < y_\alpha \implies m_4 < m^* \implies \lambda_1 = f(m_4) > 1, \tag{44a}$$

$$y_4 > y_\alpha \implies m_4 > m^* \implies \lambda_1 = f(m_4) < 1. \tag{44b}$$

As in our analysis for E_2, note that y_α is the y-intercept of the zero-growth isocline $f(m) = 1$, while y_3 and y_4 are the y-intercepts of the two zero-growth isoclines where $g(n) = 1$. We can again obtain the magnitude of λ_1 for both E_3 and E_4 directly from the configuration of the zero-growth isoclines for a particular case.

Turning to $\lambda_2 = 1 + y_i g'(y_i)$, $i = 3$ or 4, we have shown that $\lambda_2 > 0$ for E_3 (Eq. 30) and E_4 (Eq. 31). At E_3, $y = n_1^*$ and $g'(n_1^*) > 0$. Thus, $\lambda_2 > 1$ at E_3. Conversely, at E_4, $y = n_2^*$ and $g'(n_2^*) < 0$, so $\lambda_2 < 1$ at E_4.

The natures of the equilibrium points E_3 and E_4 depend on their respective λ_1. For E_3, $\lambda_2 > 1$, so E_3 is an unstable node if the lower nontrivial climax zero-growth isocline intercepts the y-axis below the nontrivial pioneer zero-growth isocline ($y_3 < y_\alpha$), and is a saddle point if the lower nontrivial climax zero-growth isocline intercepts the y-axis above the nontrivial pioneer zero-growth isocline ($y_3 > y_\alpha$).

For E_4, $0 < \lambda_2 < 1$, so E_4 is a saddle point if the upper nontrivial climax zero-growth isocline intercepts the y-axis below the nontrivial pioneer zero-growth isocline ($y_4 < y_\alpha$), and is a stable node if the upper nontrivial climax zero-growth isocline intercepts the y-axis above the nontrivial pioneer zero-growth isocline ($y_4 > y_\alpha$). See Fig. 2 and Fig. 3 for illustration. The stability of E_3 and E_4 for each of the nine cases is summarized in Table 3.

Appendix C Stability of Interior Fixed Points

We now turn to the stability of the two interior fixed points E_5 and E_6, given by Eq. 17 and Eq. 18. Rather than examining each fixed point separately and handling all cases for a particular fixed point at once, as in Appendix B, it is simpler to organize this section by individual case. The stability analyses proceed by checking the three Jury conditions (Eq. 20) for each of the six cases in which one or both interior fixed points occur. We also frequently use Descartes' Rule of Signs (Descartes, 1886) to bound the eigenvalues of the Jacobian. For convenience, we will refer to these six cases by the letter of their corresponding subfigure in Fig. 3, e.g., case *a* corresponds to Fig. 3a. Before beginning on a case-by-case basis, we present several results that simplify the overall analysis.

C.1 Conditions for Existence of Interior Fixed Points

For each of the six cases *a–f*, there are three conditions on v_1 and v_2 that must be satisfied to guarantee existence of an interior fixed point in the first quadrant. The conditions are easily derived by ensuring that both numerator and denominator are of the same sign for the pairs (x_5, y_5) and (x_6, y_6) – one condition comes from setting the numerator of the x-coordinate to be positive (negative), one condition from setting the numerator of the y-coordinate to be positive (negative), and one condition from setting the shared denominator $1 - v_1 v_2$ to be positive (negative). These conditions are presented in Table 2 and will be heavily used in proving stability of the interior fixed points. From now on, when we say that an interior fixed point exists, we are specifically referring to an interior fixed point that exists inside the first quadrant, i.e., $x > 0$ and $y > 0$.

C.2 Descartes' Rule of Signs

In addition to the conditions from Table 2, we make liberal use of Descartes' Rule of Signs (Descartes, 1886) throughout our analyses, and provide a brief refresher on this useful technique here. Consider the characteristic polynomial for the Jacobian given by

$$\chi(\lambda) = \lambda^2 - \tau\lambda + \Delta, \tag{45}$$

whose roots are the eigenvalues of Jacobian (19) and where the coefficients τ and Δ are the trace and determinant of the Jacobian. According to Descartes' Rule of Signs, the number of positive real roots of Eq. 45 — and therefore positive real eigenvalues of the Jacobian — is equal to the number of sign changes between consecutive coefficients of the polynomial, or less than it by some even number (Descartes, 1886). Thus, if there are two sign changes, we have either two or zero positive roots.

In addition, we can find the number of negative real roots of the characteristic polynomial by counting the number of sign changes in the coefficients of

$$\chi(-\lambda) = \lambda^2 + \tau\lambda + \Delta, \tag{46}$$

Again, the number of negative roots is equivalent to the number of sign changes or less by an even number, so if there are two sign changes in Eq. 46, there are two or zero negative roots.

By introducing a change of variable, we can use Descartes' Rule of Signs once more to check how many roots are greater than $+1$, simplifying the stability analysis for several cases. To analyze eigenvalues around $+1$, we introduce the shift

$$\mu = \lambda - 1 \implies \lambda = 1 + \mu. \tag{47}$$

Substituting this into Eq. 45, we obtain

$$\chi(\mu) = \mu^2 + (2 - \tau)\mu + (1 - \tau + \Delta), \tag{48}$$

and note that the constant term is the same as the left-hand side of the first Jury condition (Eq. 20a). Thus, any roots $\mu > 0$ correspond to $\lambda > 1$.

C.3 General Results for τ and Δ

Finally, we present a few useful quantities and relationships pertaining to the interior fixed points. These are summarized in Table 4. In particular, we examine the trace τ and determinant Δ of Jacobian (19), and use the results of our examination to simplify the first and second Jury conditions as well as to bound the eigenvalues of the Jacobian for both interior fixed points.

Recall that for both interior fixed points E_5 and E_6, $f(m) = 1$, $g(n) = 1$, and $m = m^*$ after substituting in the

Table 4 Quantities and relationships frequently used in Descartes' Rule of Signs or in checking the Jury conditions

Fixed point	m	n	$f(m)$	$g(n)$	$f'(m)$	$g'(n)$	τ	Δ	Sign changes in $\chi(\lambda)$	Sign changes in $\chi(-\lambda)$
E_5	m^*	n_1^*	1	1	<0	>0	>0	>0	2	0
E_6	m^*	n_2^*	1	1	<0	<0	>0	>0	2	0

explicit forms of the equilibria. For E_5, $n = n_1^*$ and for E_6, $n = n_2^*$ after substitution of the equilibria.

We can write the trace of the Jacobian, τ, as

$$\tau = 2 + xf'(m) + yg'(n), \tag{49}$$

Note that τ is positive for the Jacobian evaluated at both E_5 and E_6, as we have shown that both $1 + xf'(m) > 0$ and $1 + yg'(n) > 0$ for E_5 and E_6 (Eq. 28, Eq. 32, Eq. 33).

The determinant of the Jacobian, Δ, can be written as

$$\Delta = \left[1 + xf'(m)\right]\left[1 + yg'(n)\right] - v_1\, v_2\, x\, y\, f'(m)\, g'(n) \tag{50}$$

for $(x,y) = (x_5,y_5)$ or (x_6,y_6).

It is clear that $\Delta > 0$ when the Jacobian is evaluated at E_5. By the results of Eq. 28 and Eq. 32, the first two terms of Eq. 50 are positive, and therefore their product is positive. At E_5, $g'(n) > 0$, and thus the entire third term of Eq. 50, $[-v_1\, v_2\, x\, y\, f'(m)\, g'(n)]$, is positive. Therefore, $\Delta > 0$ at E_5.

It is not as straightforward to show that $\Delta > 0$ when the Jacobian is evaluated at E_6, but this is indeed true for all four cases *c*–*f* in which E_6 exists. We rewrite the determinant from Eq. 50, plugging in the explicit fixed point coordinates given in Eq. 18 and simplified derivatives from Eq. 22 and Eq. 24. After expanding and finding a common denominator, then rearranging and grouping like terms, we obtain the very long expression

$$\Delta = \frac{(v_1v_2 - 1) + b_2 n_1^*(m^*v_1 - n_2^*) + b_2 v_1 n_2^*(v_2 n_2^* - m^*)}{(1 + am^*)\left[1 + b_2\left(n_2^*\right)^2\right](v_1v_2 - 1)} + \frac{av_2(m^*v_1 - n_2^*) + ab_2 n_1^* n_2^* v_2(v_1 m^* - n_2^*)}{(1 + am^*)\left[1 + b_2\left(n_2^*\right)^2\right](v_1v_2 - 1)}. \tag{51}$$

In cases *c* and *e*, we see from condition three in Table 2 that the denominator of Eq. 51 is positive. Thus, we require the numerator be positive in these two cases for $\Delta > 0$. First, note that all quantities multiplying each parenthetical term are positive (this is true for all four cases *c*–*f*). Each parenthetical quantity in the numerator is in fact a condition from Table 2, and so we know the signs of these quantities. From the first condition for cases *c* and *e*, $m^*v_1 - n_2^* > 0$, from the second, $v_2 n_2^* - m^* > 0$, and we have already used the third condition. Thus, the numerator is also positive, and $\Delta > 0$ for the Jacobian evaluated at E_6 in cases *c* and *e*.

For cases *d* and *f*, the third condition from Table 2 shows that the denominator of Eq. 51 is negative, so we would like to show that the numerator is negative for $\Delta > 0$. As with cases *c* and *e*, each parenthetical quantity corresponds to a condition from Table 2, and we now know $m^*v_1 - n_2^* < 0$ and $v_2 n_2^* - m^* < 0$, in addition to the third condition we have already used. Thus, the numerator is a sum of negative quantities, and is therefore negative. Once again, $\Delta > 0$ for the Jacobian evaluated at E_6 in cases *d* and *f*.

Given that $\tau > 0$ and $\Delta > 0$ for the Jacobian evaluated at both E_5 and E_6, the second Jury condition $1 + \tau + \Delta > 0$ will clearly always be satisfied for both interior fixed points for all cases *a*–*f* (assuming the interior fixed point exists).

Additionally, observe that $\tau > 0$ and $\Delta > 0$ means there are two sign changes between coefficients in Eq. 45 and zero sign changes in Eq. 46. Therefore, by Descartes' Rule of Signs, there are zero negative eigenvalues and either two or zero positive eigenvalues of the Jacobian. Thus, for both interior fixed points in all cases *a* through *f* (assuming the interior fixed point exists), all real eigenvalues are positive. Furthermore, we either have two real, positive eigenvalues, or a pair of complex-conjugate eigenvalues for both interior fixed points in all cases.

Finally, we simplify the expression for the first Jury condition using our knowledge of τ and Δ. After substituting Eq. 49 and Eq. 50 into the left-hand side of the first Jury condition (Eq. 20a), we obtain

$$1 - \tau + \Delta = x\, y\, f'(m)\, g'(n)\,(1 - v_1v_2) \tag{52}$$

for $(x,y) = (x_5,y_5)$ or (x_6,y_6). As already stated, we consider only positive equilibria (see Subsection 4.2 for a discussion of the border cases where an interior fixed point hits an axis as a parameter is varied). We know that $f'(m) < 0$ always. Thus, ascertaining whether the first Jury condition is satisfied comes down to the sign of $g'(n)$, which is positive at E_5 and negative at E_6, and the sign of $1 - v_1v_2$, which is given by condition three in Table 2. We now proceed to a case-by-case stability analysis, recalling that a summary of the general results presented in this section are found in Table 4. This information will be particularly useful when examining cases *e* and *f*.

C.4 Case A

In case a, we have one interior fixed point E_5. The first Jury condition

$$1-\tau+\Delta = x_5\, y_5\, f'(m_5)\, g'(n_5)\,(1-v_1 v_2) > 0 \tag{53}$$

by condition three in Table 2. Thus, the first Jury condition is always satisfied. We already know that the second Jury condition is always satisfied.

The third Jury condition is $\Delta < 1$. After expanding the expression for Δ from Eq. 50 we see that the third Jury condition $\Delta < 1$ is equivalent to

$$x\, f'(m) + y\, g'(n) + x\, y\, f'(m)\, g'(n)\,(1-v_1\, v_2) < 0. \tag{54}$$

This expression does not simplify further in a useful manner. Instead, we look to express the left-hand side of Eq. 54 in terms of our relative competition coefficients v_1 and v_2, and find the curve in v_1–v_2 space where $\Delta = 1$ (or Eq. 54 is equal to zero). In other words, we want to find the boundary where we violate the third Jury condition, such that crossing that boundary causes a change of stability of E_5 in case a.

To find this boundary in v_1–v_2 space, we will substitute the explicit forms of x_5 and y_5 into the left-hand side of Eq. 54. Recall from Table 4 that $m_5 = m^*$ and $n_5 = n_1^*$. As the derivatives $f'(m^*)$ and $g'(n_1^*)$ do not have v_1 or v_2 dependence, we can leave them in their general form. After this substitution and minor simplification, the boundary where we violate the third Jury condition is given by

$$\begin{aligned} 0 \;=\; & \frac{(m^* - v_2 n_1^*)\, f'(m^*)}{1-v_1 v_2} + \frac{(n_1^* - v_1 m^*)\, g'(n_1^*)}{1-v_1 v_2} \\ & + \frac{(m^* - v_2 n_1^*)\,(n_1^* - v_1 m^*)\, f'(m^*)\, g'(n_1^*)}{1-v_1 v_2}. \end{aligned} \tag{55}$$

From condition three in Table 2, we know $1 - v_1 v_2 \neq 0$ while in this case, and so we safely multiply both sides by $1 - v_1 v_2$ to obtain

$$\begin{aligned} 0 \;=\; & (m^* - v_2 n_1^*)\, f'(m^*) + (n_1^* - v_1 m^*)\, g'(n_1^*) \\ & + (m^* - v_2 n_1^*)\,(n_1^* - v_1 m^*)\, f'(m^*)\, g'(n_1^*). \end{aligned} \tag{56}$$

Rearranging and solving for v_2 as a function of v_1 gives us the curve

$$\begin{aligned} v_2 = h(v_1) = & \frac{v_1 \left[m^* g'(n_1^*) + (m^*)^2 f'(m^*)\, g'(n_1^*) \right]}{n_1^* f'(m^*) \left[v_1 m^* g'(n_1^*) - n_1^* g'(n_1^*) - 1 \right]} \\ & - \frac{m^* f'(m^*) + n_1^* g'(n_1^*) + m^* n_1^* f'(m^*)\, g'(n_1^*)}{n_1^* f'(m^*) \left[v_1 m^* g'(n_1^*) - n_1^* g'(n_1^*) - 1 \right]}. \end{aligned} \tag{57}$$

While Eq. 57 does not simplify further, it should be noted that all quantities are constants except for v_1 and v_2, assuming that all other parameters are held constant. Thus, $v_2 = h(v_1)$ from Eq. 57 gives us the boundary of the region in v_1–v_2 space where E_5 satisfies the third Jury condition (see Fig. 4a).

We will briefly note that this curve does yield both a vertical and horizontal asymptote. The vertical asymptote occurs at

$$v_1 = v_1^* = \frac{n_1^* g'(n_1^*) + 1}{m^* g'(n_1^*)} \tag{58}$$

and the horizontal asymptote at

$$v_2 = v_2^* = \frac{m^* f'(m^*) + 1}{n_1^* f'(m^*)}. \tag{59}$$

Eq. 57 therefore has two branches. The left branch is valid for $v_1 < v_1^*$ and $v_2 > v_2^*$, and the right branch is valid for $v_1 > v_1^*$ and $v_2 < v_2^*$, with v_1^* and v_2^* given by Eq. 58 and Eq. 59. However, note that

$$v_2^* = \frac{m^* f'(m^*) + 1}{n_1^* f'(m^*)} = \frac{m^*}{n_1^*} + \frac{1}{n_1^* f'(m^*)} < \frac{m^*}{n_1^*}. \tag{60}$$

Recall by condition two from Table 2 that case a requires $v_2 > \frac{m^*}{n_1^*}$. Therefore, the right branch of Eq. 57, for which $v_2 < v_2^* < \frac{m^*}{n_1^*}$ is not a valid solution for this parameter regime, and so we only consider the left branch of Eq. 57 when determining the region of stability for E_5. On one side of the left branch of $v_2 = h(v_1)$, E_5 is stable, and on the other side of the curve E_5 is unstable.

C.5 Case B

In case b, we have the same interior fixed point E_5 as in case a. For the first Jury condition, we see that the third condition from Table 2 is reversed, and

$$1-\tau+\Delta = x_5\, y_5\, f'(m_5)\, g'(n_5)\,(1-v_1 v_2) < 0. \tag{61}$$

The first Jury condition is never satisfied. By failing the first Jury condition, we know there must be at least one eigenvalue $\lambda_1 > 1$. We can confirm this by examining the shifted characteristic polynomial in Eq. 48. By our above analysis, we know the constant term $1-\tau+\Delta < 0$, so no matter the sign of $2-\tau$, the coefficient of the linear term, there will be one sign change between consecutive coefficients in Eq. 48. Therefore we have one positive real root μ_1, and thus only one eigenvalue $\lambda_1 > 1$.

We have already demonstrated that in general, if the eigenvalues associated with an interior fixed point are real, they will both be positive. As we have one real λ, both must be real, as complex eigenvalues come in pairs. We therefore have $\lambda_1 > 1$, $0 < \lambda_2 < 1$, and thus E_5 is a saddle point in case b.

C.6 Case C

In case c, we have one interior fixed point E_6. As in case b, the first Jury condition is never satisfied as

$$1-\tau+\Delta = x_6\, y_6\, f'(m_6)\, g'(n_6)\,(1-v_1 v_2) < 0 \tag{62}$$

using the third condition from Table 2. Precisely as before, we will use Descartes' Rule of Signs to bound our eigenvalues. We have at least one eigenvalue $\lambda_1 > 1$, by the results of the first Jury condition. To determine if both eigenvalues are larger than $+1$, we examine the shifted characteristic polynomial (Eq. 48). As before, we know the constant term $1-\tau+\Delta < 0$, so no matter the sign of $2-\tau$, there is one sign change between the polynomial coefficients. Thus, there is one positive real root μ_1, and therefore only one root $\lambda_1 > 1$. Given one real λ, the other eigenvalue must be real as well, and we know all real eigenvalues are positive for the interior fixed points. Thus, $\lambda_1 > 1$, $0 < \lambda_2 < 1$, and E_6 is a saddle point for case c.

C.7 Case D

In case d, we have the same interior fixed point E_6 as in case c. Using the third condition from Table 2, we now see

$$1-\tau+\Delta = x_6\, y_6\, f'(m_6)\, g'(n_6)\,(1-v_1 v_2) > 0, \tag{63}$$

and the first Jury condition is always satisfied in this case. The second Jury condition is also always satisfied.

Rather than checking the third Jury condition $\Delta < 1$, we instead show that both eigenvalues are real and bounded between 0 and $+1$. This is evidently sufficient to classify the fixed point, and proving realness eliminates the need to check the third Jury condition, which tests complex eigenvalues.

Consider the generalized eigenvalues of the Jacobian matrix evaluated at E_6, which are the roots of the characteristic polynomial Eq. 45:

$$\lambda_{1,2} = \frac{\tau \pm \sqrt{\tau^2 - 4\Delta}}{2}. \tag{64}$$

If $\tau^2 - 4\Delta > 0$, then both eigenvalues are real. Using the trace from Eq. 49 and the expanded form of the determinant in Eq. 50, after combining like terms we find

$$\begin{aligned}\tau^2 - 4\Delta &= \left[x_6 f'(m_6)\right]^2 + \left[y_6 g'(n_6)\right]^2 - 2x_6 y_6 f'(m_6)\, g'(n_6) \\ &\quad + 4v_1 v_2 x_6 y_6 f'(m_6)\, g'(n_6) \\ &= \left[x_6 f'(m_6) - y_6 g'(n_6)\right]^2 \\ &\quad + 4v_1 v_2 x_6 y_6 f'(m_6)\, g'(n_6) > 0,\end{aligned} \tag{65}$$

as both terms are clearly positive under the conditions of this case. In fact, that this holds for E_6 for any parameter regime, as we are not using conditions pertaining to a particular case, only conditions that are true at E_6. Thus, both eigenvalues are real for all cases where E_6 exists.

Having proved the eigenvalues are real, we again use Descartes' Rule of Signs to bound the eigenvalues. By our earlier result from Appendix C.3, since our eigenvalues are real we must have two positive eigenvalues, $\lambda_{1,2} > 0$.

We will use the shifted characteristic polynomial (Eq. 48) to determine if $\lambda_{1,2} > 1$. By the first Jury condition, we know the constant term $1-\tau+\Delta > 0$. The coefficient of the linear term

$$2-\tau = -x_6 f'(m_6) - y_6 g'(n_6) > 0, \tag{66}$$

as both derivatives are negative at E_6. All coefficients of Eq. 48 are therefore positive, so there are zero sign changes and zero roots $\mu > 0$, meaning there are no eigenvalues $\lambda > 1$ (by Eq. 47). Thus, $0 < \lambda_{1,2} < 1$, and E_6 is a stable node in case d.

C.8 Case E

In case e, we have both interior fixed points E_5 and E_6. We will first consider E_5. It is clear that

$$1-\tau+\Delta = x_5\, y_5\, f'(m_5)\, g'(n_5)\,(1-v_1 v_2) > 0 \tag{67}$$

by the conditions from Table 2 and Table 4, so the first Jury condition is always satisfied for E_5 in case e. The second Jury condition is also always satisfied for E_5 in case e.

The third Jury condition is $\Delta < 1$. The expression for the third Jury condition is precisely the same as Eq. 54 from Appendix C.4, and indeed the entirety of the analysis is identical to analysis of the third Jury condition for E_5 from case a. We do not repeat it here, and refer the reader back to Appendix C.4 for details. Instead, we will simply recall that we can express the boundary of the region of stability for E_5 in terms of v_1 and v_2. This yields a rational function, given by Eq. 57, with two branches. As the bounds on v_2 are the same between case a and case e (see Table 2), only the left branch is valid for determining the boundary of the region of stabiliy in case e. To one side of this branch, E_5 is stable, and on the other side E_5 is unstable. See Fig. 4b for illustration of the region of stability for E_5 in case e.

We now turn to the second interior fixed point, E_6. We see that

$$1-\tau+\Delta = x_6\, y_6\, f'(m_6)\, g'(n_6)\,(1-v_1 v_2) < 0, \tag{68}$$

by the conditions from Table 2 and Table 4, so the first Jury condition is never satisfied for E_6 in case e.

As should now be familiar, we will use Descartes' Rule of Signs to bound the eigenvalues. By the results of analyzing the first Jury condition, there is at least one eigenvalue larger than $+1$. Examining the shifted characteristic polynomial (Eq. 48), we see there is only one sign change between the polynomial's coefficients no matter the sign of $2-\tau$, as the constant term $1-\tau+\Delta<0$. There is one positive real root μ_1, and thus only one eigenvalue $\lambda_1>1$. The other eigenvalue λ_2 must also be real, and as all real eigenvalues are positive for interior fixed points, we know $\lambda_1>1$, $0<\lambda_2<1$. Therefore, E_6 is a saddle point for case *e*.

C.9 Case F

In case *f*, we again have both interior fixed points E_5 and E_6. We first consider E_5.

Using the conditions and relationships in Table 2 and Table 4,

$$1-\tau+\Delta=x_5\,y_5\,f'(m_5)\,g'(n_5)\,(1-v_1v_2)<0. \tag{69}$$

The first Jury condition is never satisfied for E_5 in case *f*. Considering the shifted polynomial Eq. 48, there is one sign change between coefficients of the polynomial and therefore one root $\mu_1>0$. Thus, we have only one eigenvalue $\lambda_1>1$. As before, the second eigenvalue λ_2 must be real given that λ_1 is real, and we know all real eigenvalues of the interior fixed points are positive. We find that $\lambda_1>1$, $0<\lambda_2<1$, and E_5 is a saddle point for case *f*.

Finally, we consider E_6 for this final case. The first Jury condition is obviously always satisfied as

$$1-\tau+\Delta=x_6\,y_6\,f'(m_6)\,g'(n_6)\,(1-v_1v_2)>0 \tag{70}$$

for E_6 in case *f*, by the conditions from Table 2 and Table 4. The second Jury condition is always satisfied.

As with case *d*, we will bound the eigenvalues between 0 and $+1$ rather than checking the third Jury condition. Recall that in the stability analysis for case *d*, we demonstrated that both eigenvalues associated with E_6 are real for all cases where E_6 exists. Thus, we already know our eigenvalues to be real for E_6 in case *f*.

Employing the oft-used result a final time, we know that since the eigenvalues for E_6 are real, we have $\lambda_{1,2}>0$. Identically to the analysis for case *d*, we consider the shifted characteristic polynomial Eq. 48. As the first Jury condition is always satisfied for E_6 in this case, the constant term $1-\tau+\Delta>0$. It is evident that the coefficient of the linear term

$$2-\tau=-x_6f'(m_6)-y_6g'(n_6)>0 \tag{71}$$

as well. There are zero sign changes between coefficients and therefore zero roots $\mu>0$. Thus, there are no eigenvalues $\lambda>1$ (by Eq. 47). With this result, we see that $0<\lambda_{1,2}<1$, and E_6 is a stable node in case *f*.

The results of the above stability analyses for all six cases with one or more interior fixed point in the first quadrant are summarized in Table 3. This completes our analytic stability analysis; analyses of the global bifurcations present in cases *a* and *e* were performed numerically.

Figures

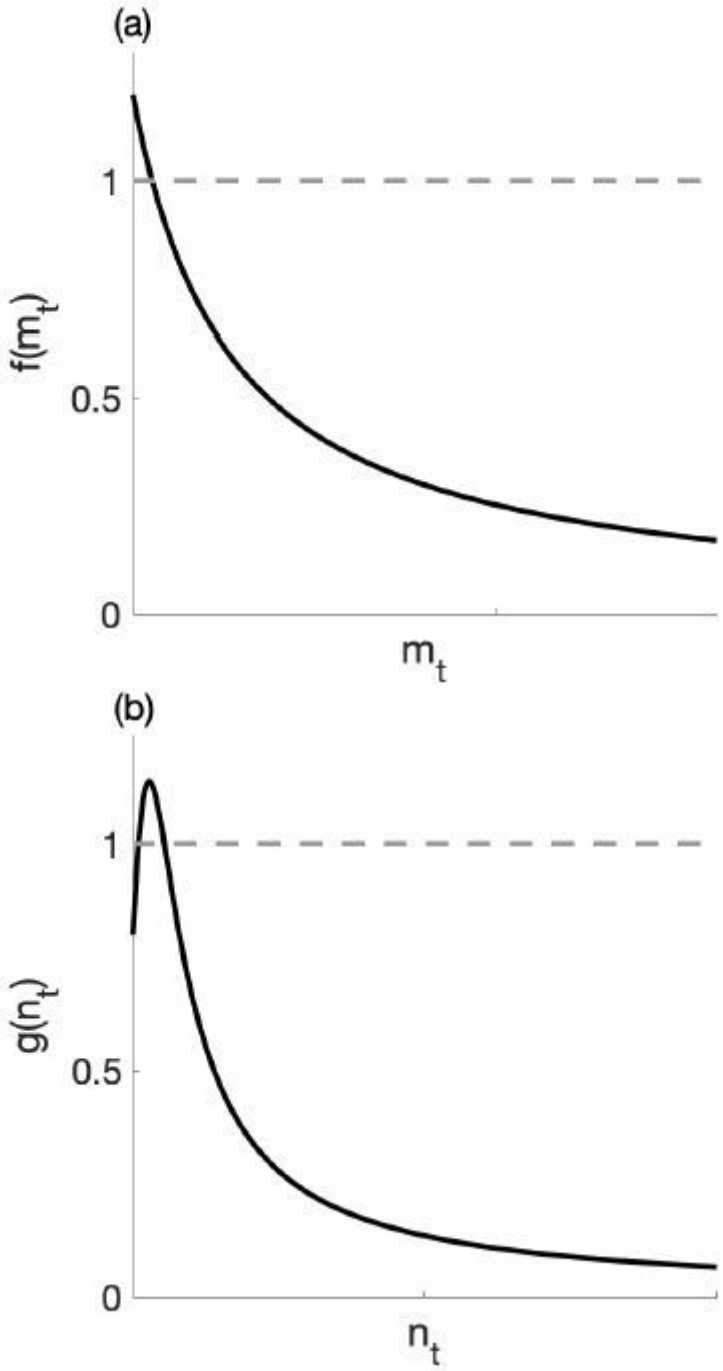

Figure 1

Fitness functions for both species from the nondimensionalized model. a, the pioneer species' fitness function f (mt). b, the climax species' fitness function g(nt). The horizontal dashed gray lines indicate where the fitness function is equal to one, where the root(s) of the functions occur

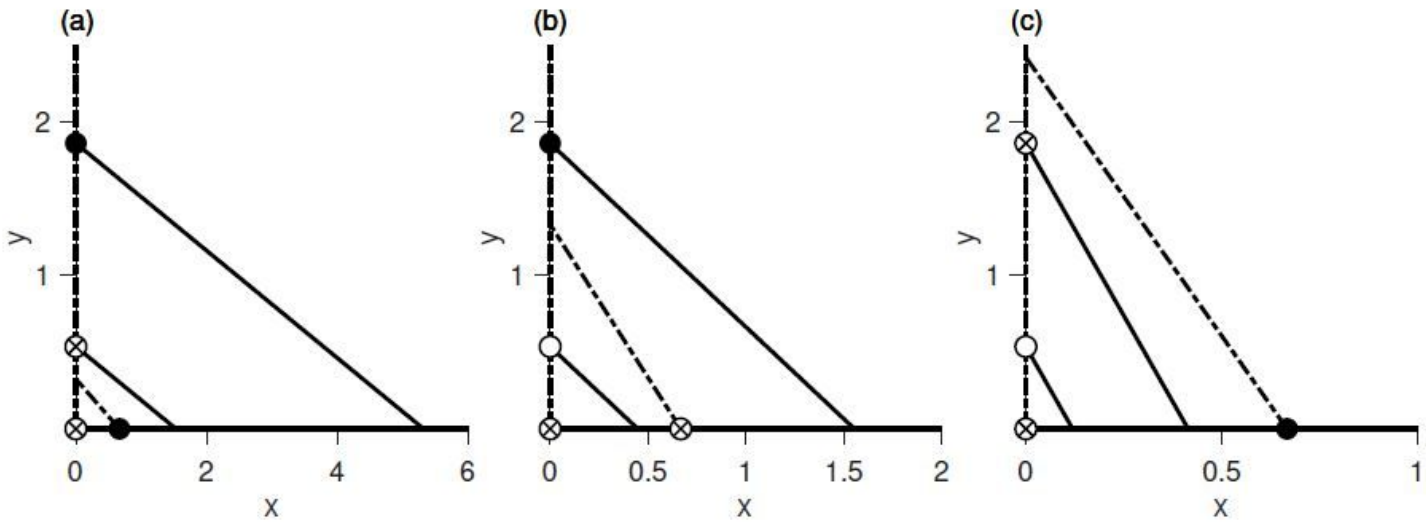

Figure 2

Zero-growth isocline orientations and stabilities of fixed points for cases where only boundary fixed points exist. The dashed-dotted lines are the pioneer species' zero-growth isoclines; solid lines (including y = 0) are the climax species' zero growth isoclines. Solid black circles indicate asymptotically stable fixed points. Circles with crosses are saddle points, while open circles signify other unstable fixed points. For all cases, parameter values are R1 = 1:2;R2 = 0:8;a = 0:3;b1 = 0:6;b2 = 0:2. a, v1 = 0:35;v2 = 2:05. b, v1 = 1:2;v2 = 0:5. c, v1 = 4:5;v2 = 0:275

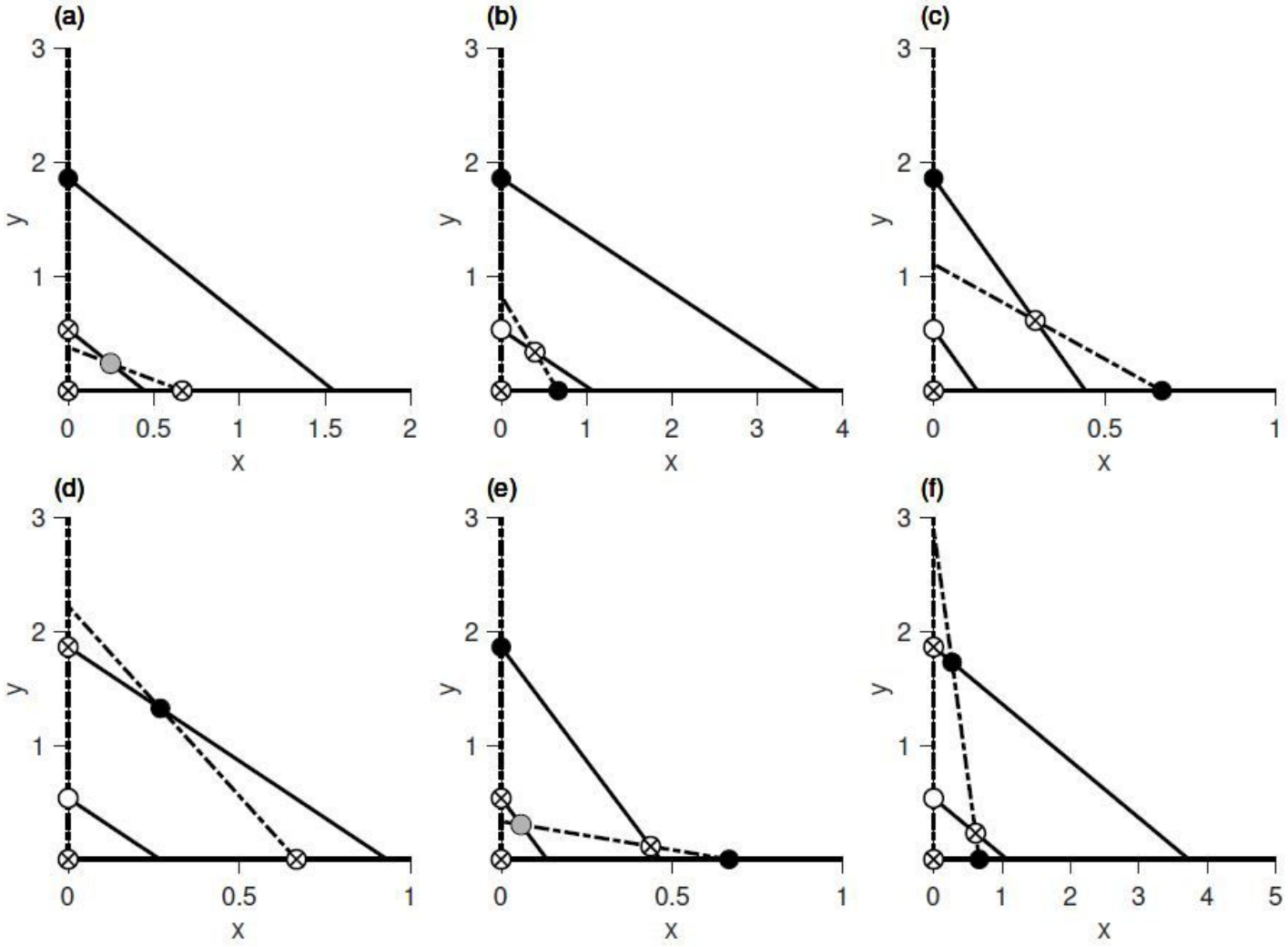

Figure 3

Zero-growth isocline configurations and stabilities of equilibria for cases where interior equilibria occur. The dashed-dotted lines are the pioneer species' zero-growth isoclines; solid lines (including y = 0) are the climax species' zero growth isoclines. Parameter values for all cases are R1 = 1:2;R2 = 0:8;a = 0:3;b1 = 0:6;b2 = 0:2. The same classification system as in Fig. 2 applies; gray shaded circles represent equilibria that undergo bifurcations. a and b, one interior equilibrium results from the crossing of the pioneer zero-growth isocline and the lower climax zerogrowth isocline. a, v1 = 1:2;v2 = 1:75; b, v1 = 0:5;v2 = 0:8. c and d, one interior equilibrium results from crossing the upper climax zero-growth isocline. c, v1 = 4:2;v2 = 0:6; d, v1 = 2;v2 = 0:3. e and f, two interior equilibria occur. e, v1 = 4;v2 = 2; f, v1 = 0:5;v2 = 0:23

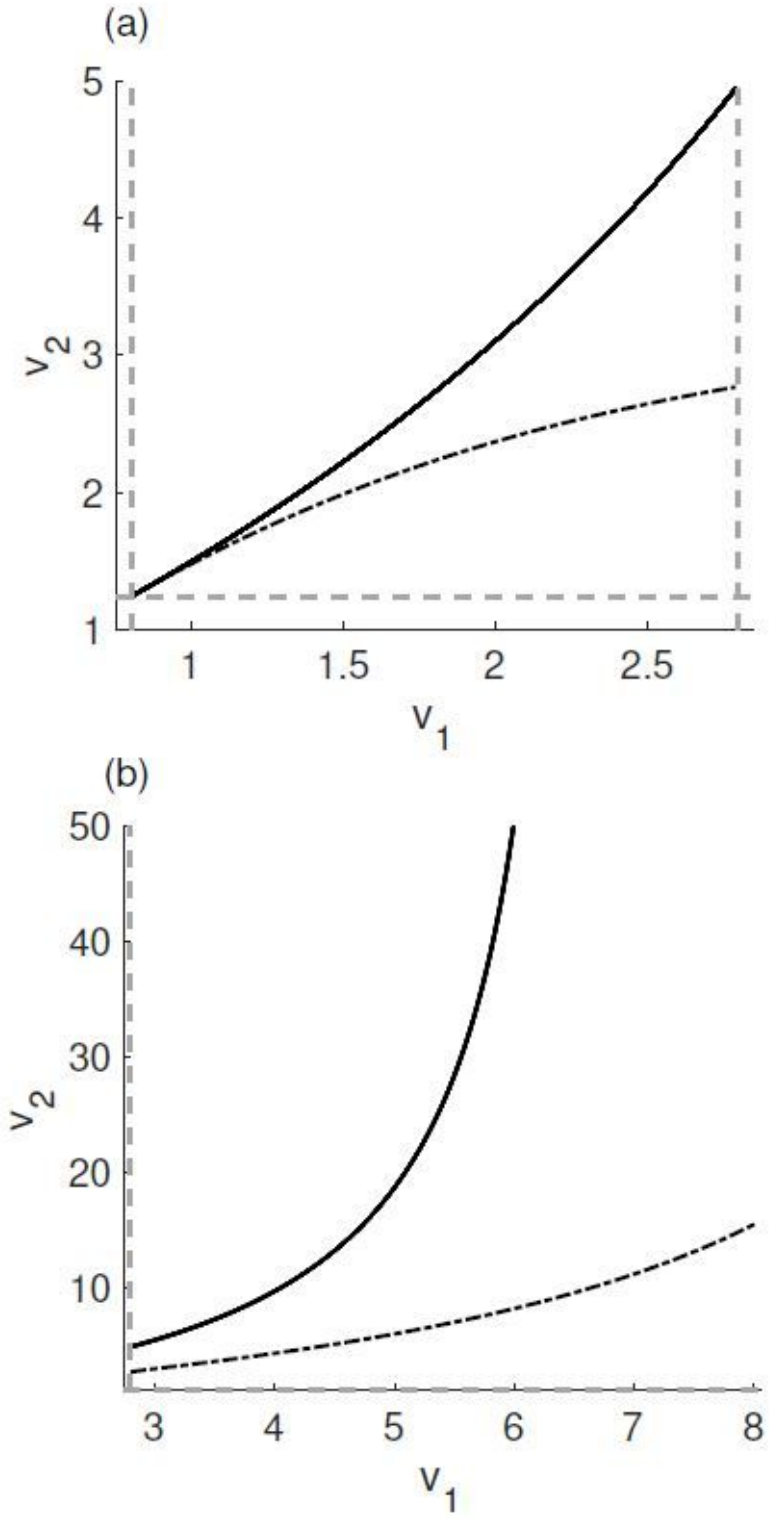

Figure 4

Stability region for equilibrium E5, defined by the curves in (v1;v2) parameter space where bifurcations occur. In both cases, E5 is stable for parameter values above and to the left of the solid curve given by D = 1; crossing this curve results in a loss of stability via a Neimark–Sacker bifurcation and the birth of an invariant circle. The lower dashed-dotted curves are the boundaries at which the global bifurcations occur; crossing the dashed-dotted curve results in the abrupt disappearance of the invariant circle. a, the

first case corresponding to Fig. 3a with a heteroclinic bifurcation. The global bifurcation curve was found by using the bisection method to calculate, for a given v1, the v2 value for which a trajectory starting on the unstable manifold of E2 ended at, or very near to, E3, such that the unstable manifold of E2 connected with the stable manifold of E3. b, the second case corresponding to Fig. 3e with a homoclinic bifurcation. The global bifurcation curve for this case was found by using the bisection method to determine, for a given v1, the v2 value for which a trajectory starting on the unstable manifold of E6 returned to E6, such that the unstable and stable manifolds of E6 connected to form a homoclinic connection. The dashed gray lines in each panel indicate the boundaries on v1 and v2 such that we are in the appropriate geometric case, i.e., that the isoclines intersect in the appropriate configuration. Parameter values for both cases are R1 = 1:2;R2 = 0:8;a = 0:3;b1 = 0:6;b2 = 0:2

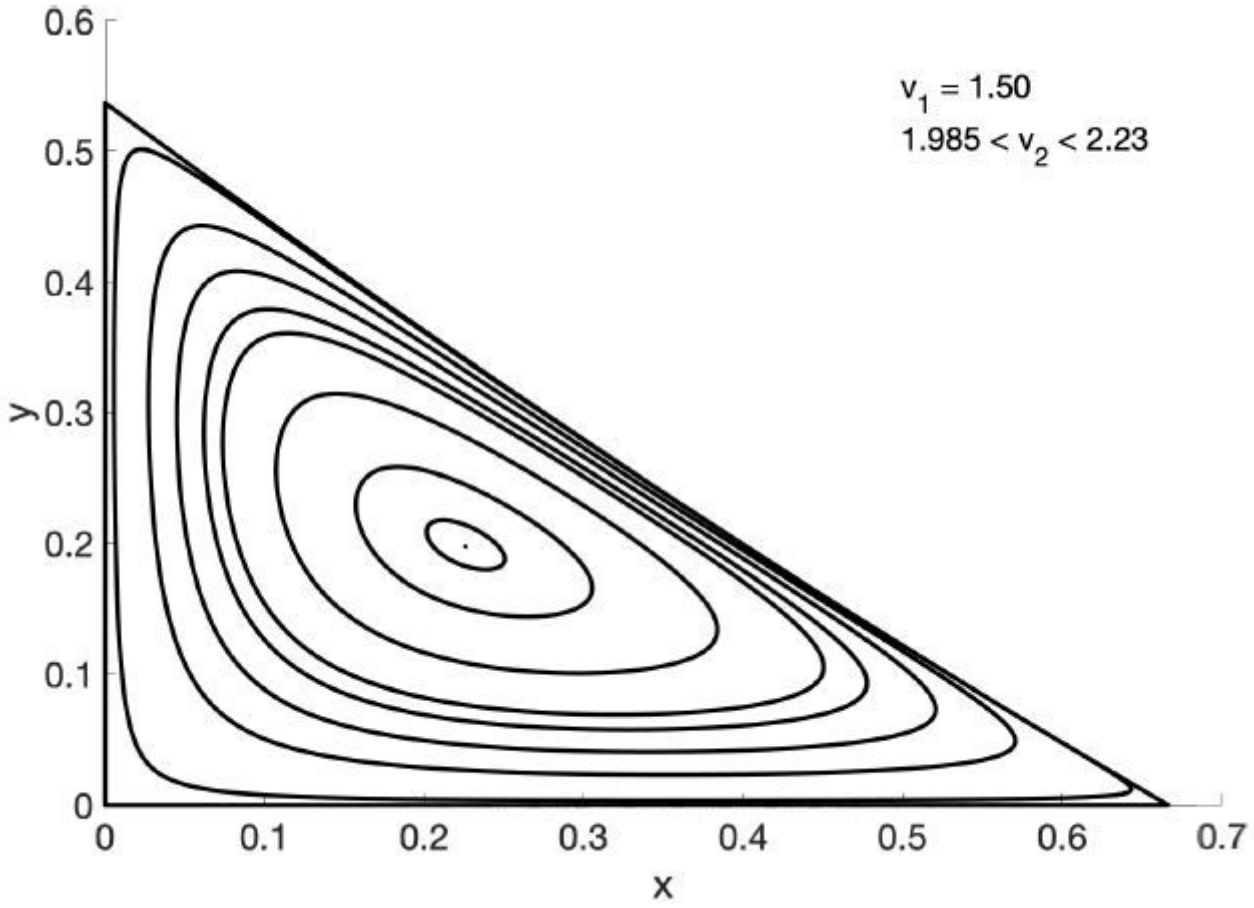

Figure 5

Growth of the invariant circle as v2 decreases from 2:23 to just above 1:985 in the first case with a Neimark–Sacker bifurcation. The point in the middle of the invariant circles is E5 for v2 = 2:23, when E5 is asymptotically stable.We ran the system for 50,000 iterations; the final 15,000 iterations were plotted for ten v2 values. Parameter values are R1 = 1:2;R2 = 0:8;a = 0:3;b1 = 0:6;b2 = 0:2

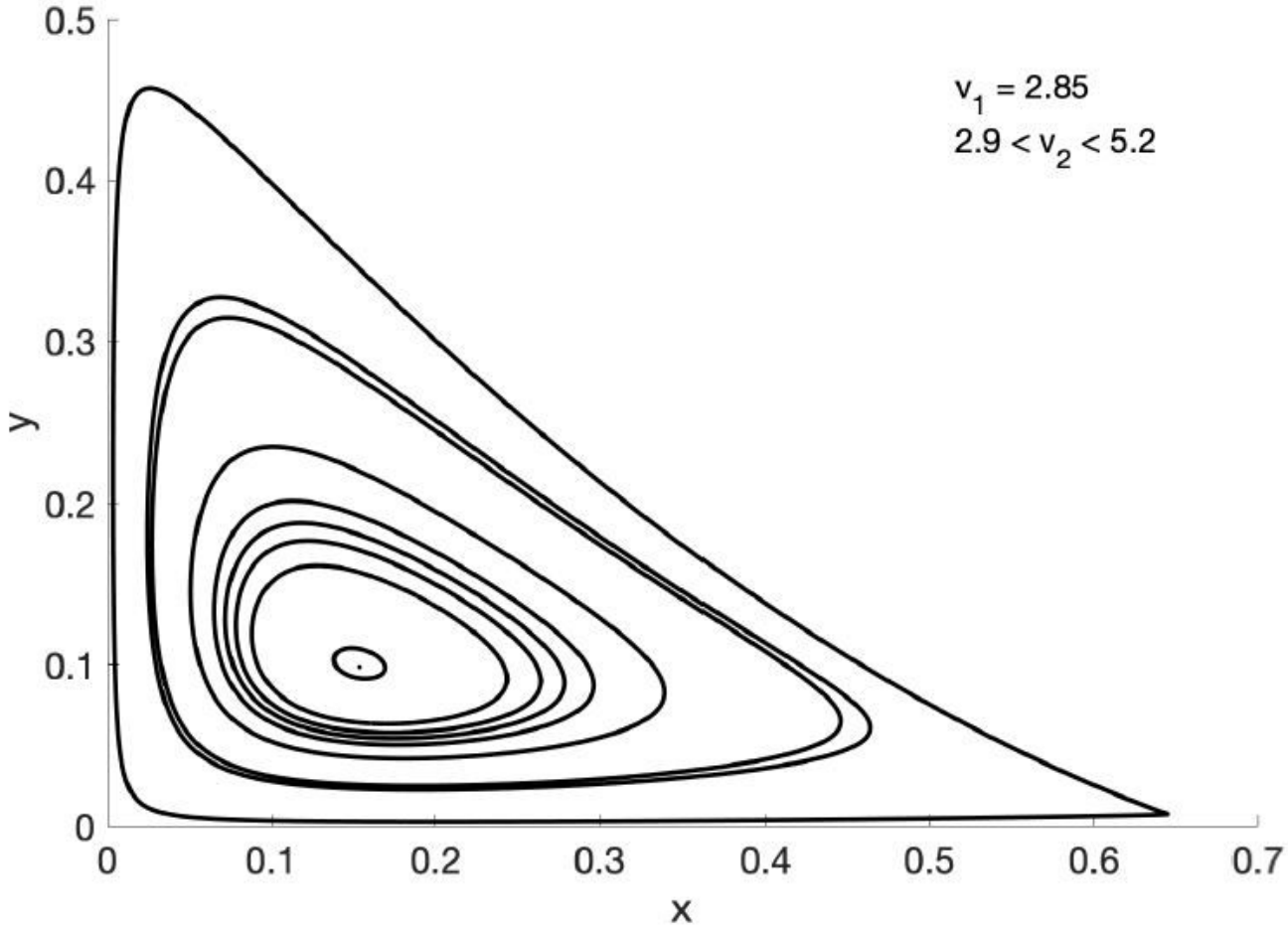

Figure 6

Growth of the invariant circle in the second case as v2 decreases from 5:2 to 2:9. The single point in the middle of the invariant circles is E5 for v2 = 5:2, when E5 is asymptotically stable. The system was run for 1,000,000 iterations; the final 200,000 iterations were plotted for ten v2 values. This number of iterations was necessary to fill in the invariant circle for some v2 values for which the system had nearly rational rotation numbers. Other parameter values are R1 = 1:2;R2 = 0:8;a = 0:3;b1 = 0:6;b2 = 0:2

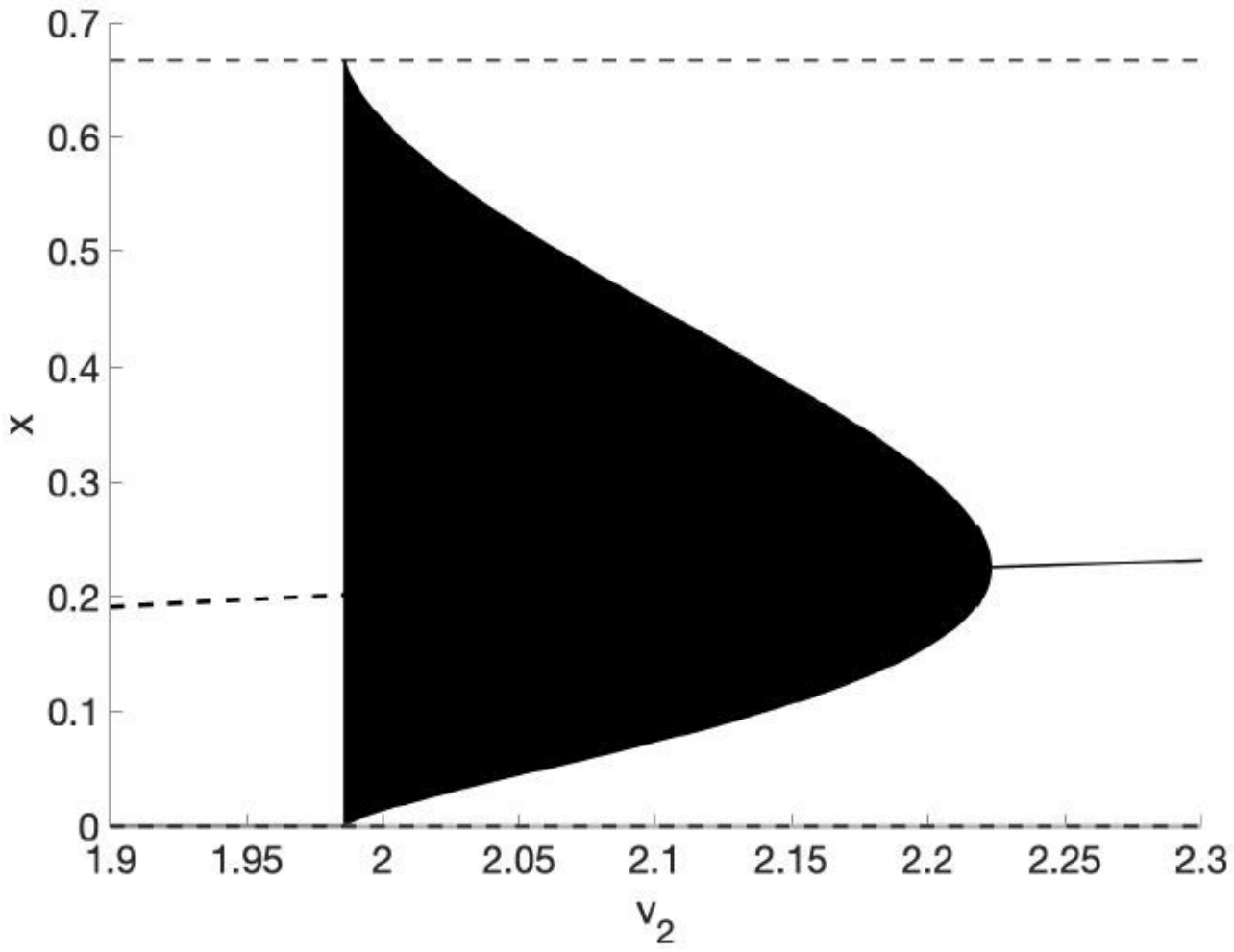

Figure 7

Bifurcation diagram for the first case with bifurcations, showing the x coordinates of the attractors and other fixed points. Dashed lines represent saddle points or other unstable fixed points; solid lines represent asymptotically stable fixed points. The black dashed line on top of the gray solid line at x = 0 is included to show there are both stable and unstable fixed points with coordinate x = 0. As v2 decreases, we see the birth of an invariant circle due to a Neimark–Sacker bifurcation. All x values on the invariant circle are mapped, such that for a single v2 value there are many values of x. The invariant circle grows as v2 decreases further until its sudden disappearance in a global bifurcation as the invariant circle runs into a heteroclinic cycle between the three saddle points of this case. Parameter values are R1 = 1:2;R2 = 0:8;a = 0:3;b1 = 0:6;b2 = 0:2;v1 = 1:5

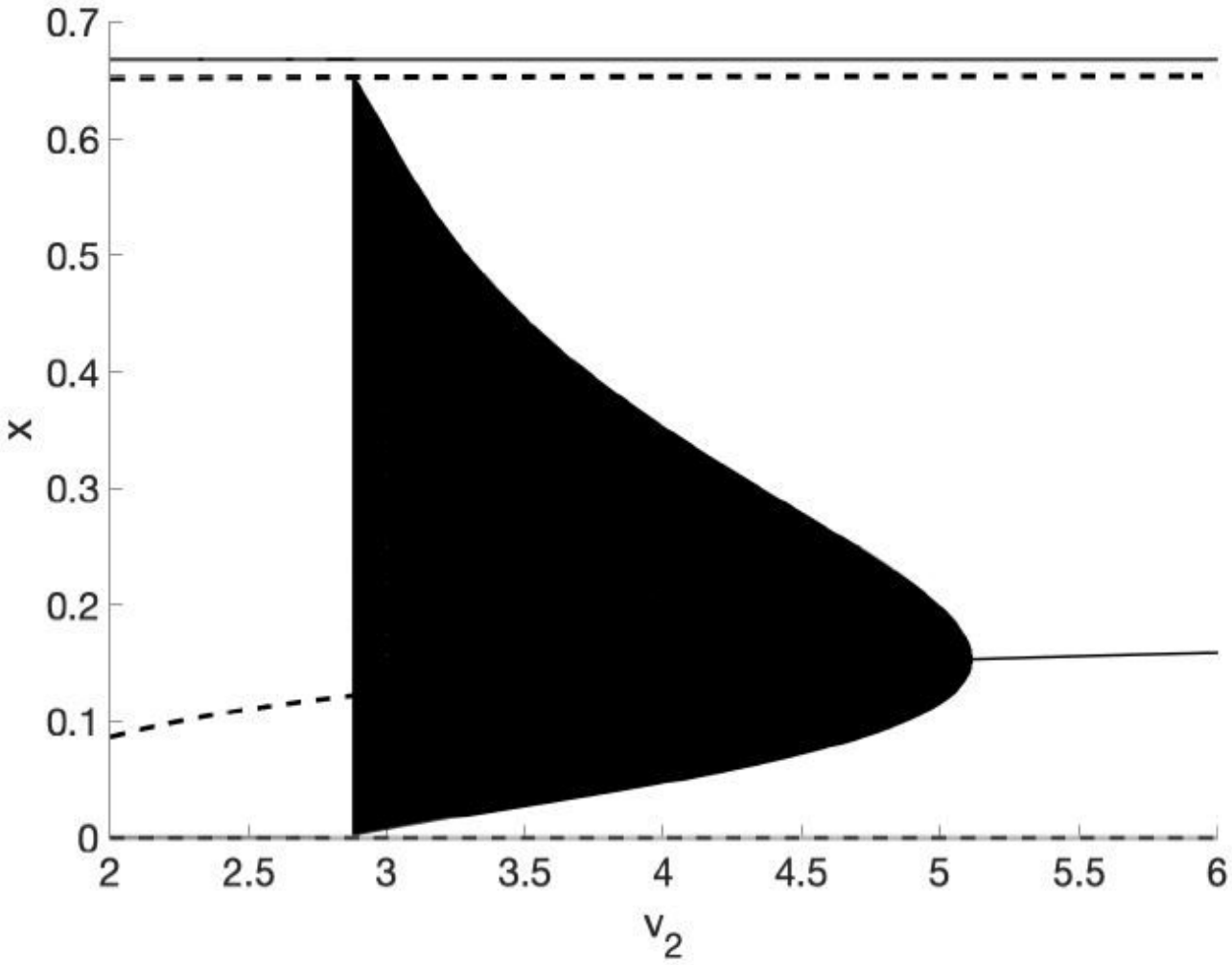

Figure 8

Bifurcation diagram of the second case showing the x coordinates of the attractors and other fixed points. Dashed lines show saddle points or other unstable fixed points; solid lines represent asymptotically stable fixed points. The black dashed line on top of the solid gray line at x = 0 shows there are both stable and unstable fixed points at x=0. As with the first case, as v2 decreases an invariant circle is born via a Neimark–Sacker bifurcation, eventually abruptly vanishing in a global bifurcation. Parameter values are R1 = 1:2;R2 = 0:8;a = 0:3;b1 = 0:6;b2 = 0:2;v1 = 2:85

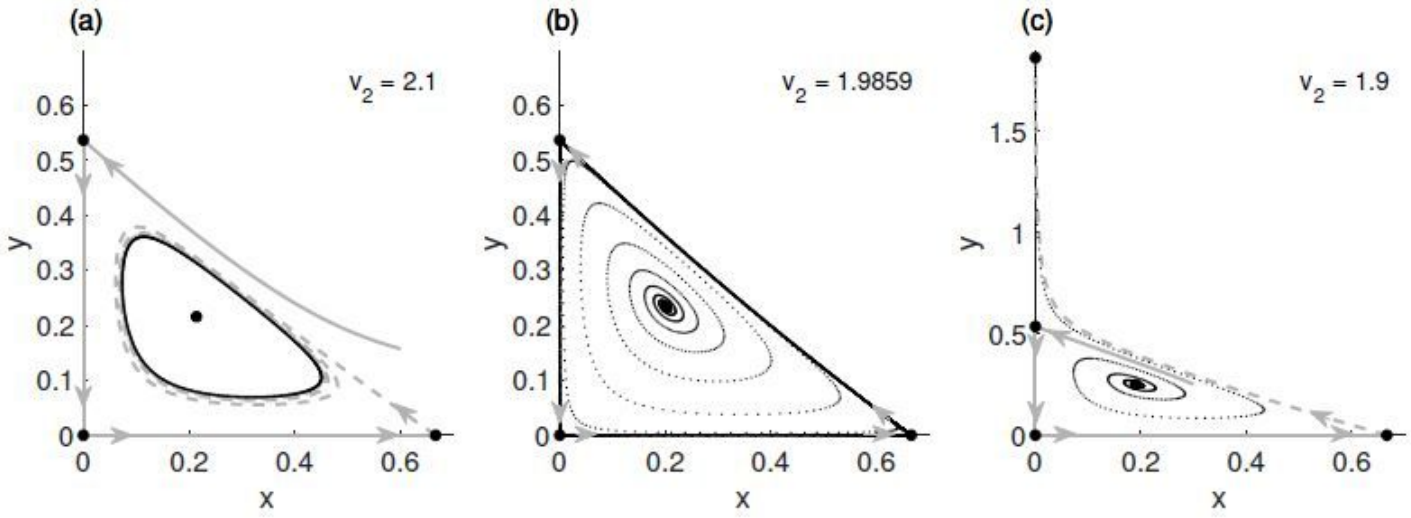

Figure 9

Behavior of the system before, at, and after the heteroclinic bifurcation in the first case with bifurcations. Solid gray lines are stable manifolds, dashed gray lines are unstable manifolds. The axes are also invariant manifolds and form heteroclinic connections between E1 and E2 on the x axis and E1 and E3 on the y axis. Large black points are equilibria, trajectories of the system with an initial condition near E5 are shown with smaller black points. The arrows indicate the direction of travel along the manifold. a, prior to the global bifurcation, the unstable manifold from E2 passes below the stable manifold of E3 and winds onto the attracting invariant circle. b, at the point of global bifurcation, a heteroclinic cycle forms and the unstable and stable manifolds of E2 and E3 link together to complete the cycle. c, after the global bifurcation, the heteroclinic connection is broken and no stable coexistence state exists. Almost all trajectories go to E4 on the y axis, save for solutions starting on the stable manifold of E3 or on the axes between E1 and E2 or between E1 and E3. Parameter values are R1 = 1:2;R2 = 0:8;a = 0:3;b1 = 0:6;b2 = 0:2;v1 = 1:5

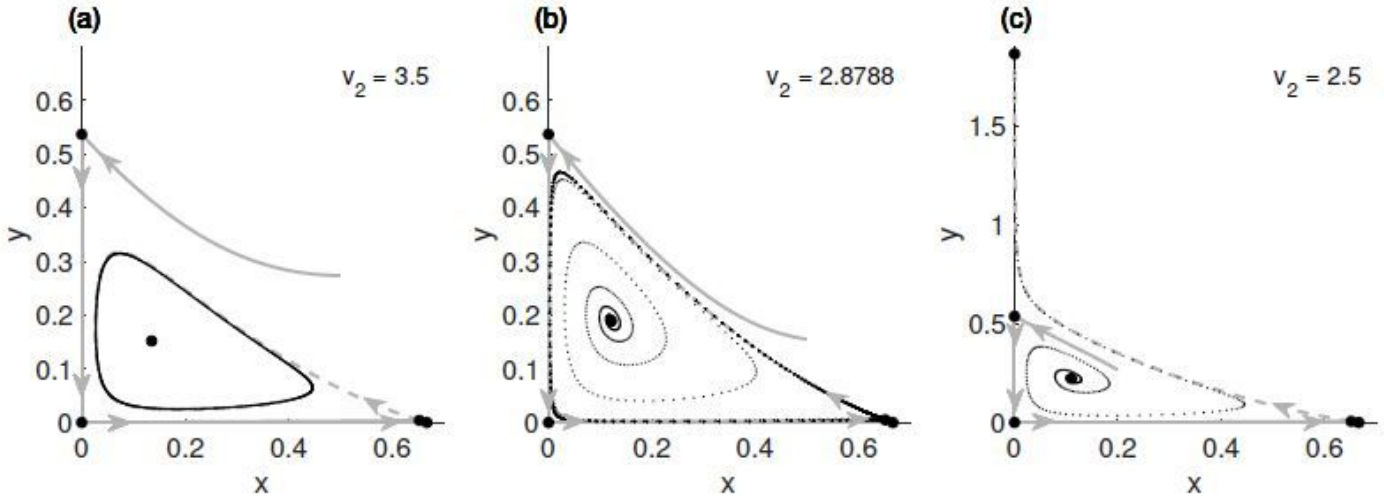

Figure 10

Behavior of the system before, at, and after the homoclinic bifurcation in the second case with bifurcations. Solid gray lines are stable manifolds, dashed gray lines are unstable manifolds. The axes are again invariant manifolds with heteroclinic connections between E1 and E2 on the x axis and E1 and E3 on the y axis. Large black points represent equilibria, trajectories of the system starting near E5 are shown with smaller black points. Arrows indicate direction of travel along the manifolds. a, prior to the global bifurcation, the unstable manifold from interior equilibrium E6 passes below the stable manifold from E3 on the y axis and winds onto the attracting invariant circle. b, at the point of global bifurcation, a homoclinic connection forms between the stable and unstable manifolds of E6, passing very close to the invariant manifolds on the axes. c, after the global bifurcation, no stable coexistence state exists and the homoclinic connection has been broken. Almost all trajectories go either to E4 on the y axis (shown here) or E2 on the x axis. Parameter values are R1 = 1:2;R2 = 0:8;a = 0:3;b1 = 0:6;b2 = 0:2;v1 = 2:85

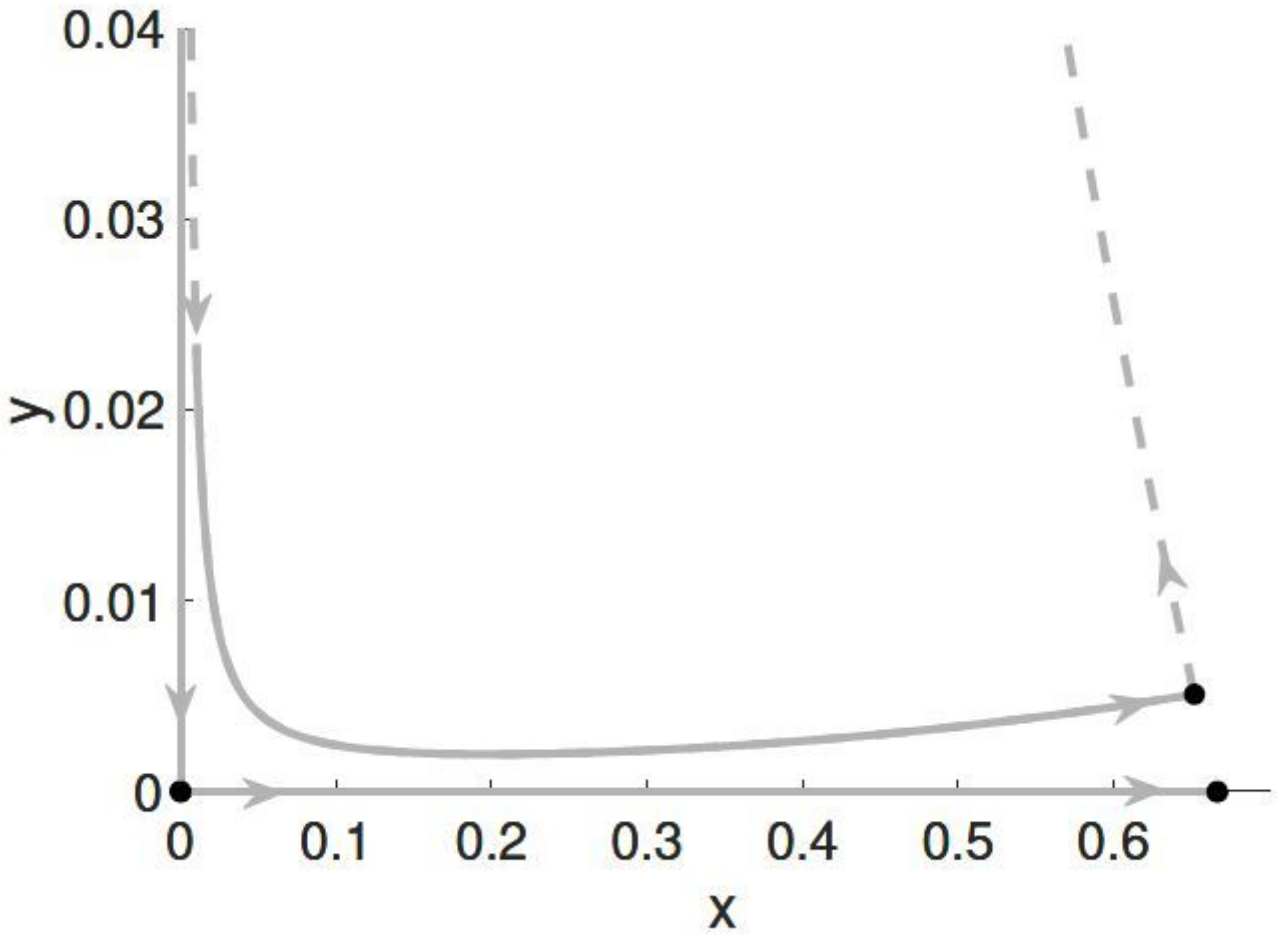

Figure 11

A magnified view of the lower part of the homoclinic connection in the second case with bifurcations. Here, the loop between the stable and unstable manifolds of E6 is clear, and we more easily see that the invariant manifolds of E6 do not intersect the manifolds on the axes of E1 or E2. Solid gray lines are stable manifolds, dashed gray lines are unstable manifolds, and points are equilibria. Arrows indicate

direction of travel along the manifolds. Parameter values are R1 = 1:2;R2 = 0:8;a = 0:3;b1 = 0:6;b2 = 0:2;v1 = 2:85; and v2 = 2:878800266186866